Resonance enhanced laser-induced breakdown spectroscopy

The design and build of a Resonance-enhanced laser-induced breakdown spectroscopy setup

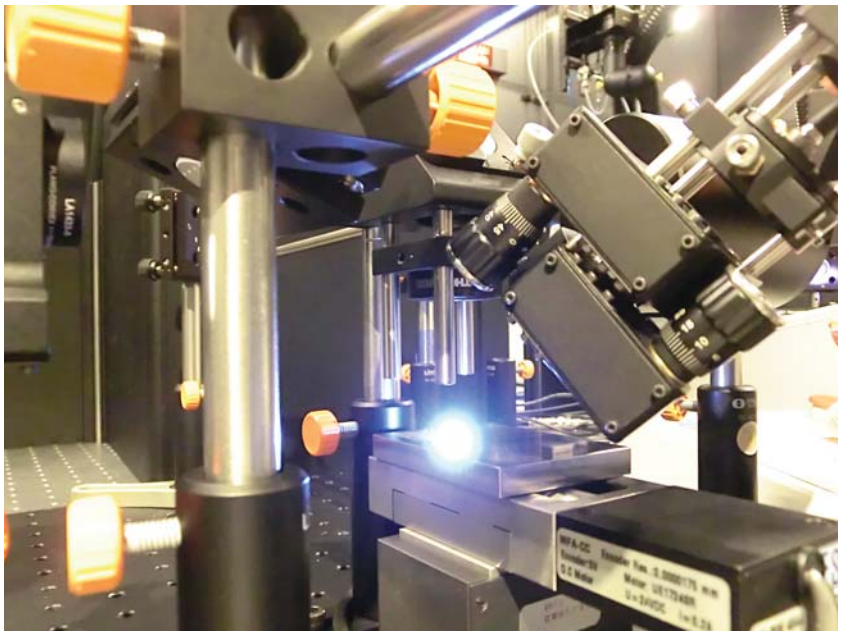

Daniël Bouman

May 31, 2013

Educational Tutor:
Dr. Ir. C. Swarts

Company supervisor:
Dr. M. Sovago
Graduation company:
TNO Optics

Abstract

Resonance-enhanced laser-induced breakdown spectroscopy was used to increase the elemental sensitivity of laser-induced breakdown spectroscopy. In resonance-enhanced laser-induced breakdown spectroscopy, two lasers are used. The first laser creates a plasma, and the second laser re excites the most abundant element. A setup is build and measurements were performed on basalt, a titanium alloy and a steel 316 alloy. An enhancement in signal-to-noise ratio of up to 7-fold was found for the titanium alloy. The influence of the quality of the beam profile was also investigated. When the excitation laser becomes ablative and a second crater is created, the resonance enhancement disappears. The signal was still enhanced but by thermal excitation, which is not as effective. Resonance-enhanced laser-induced breakdown spectroscopy was found to be very effective, but also very sensitive to spacial and temporal alignment.

Contents

Notations and abbreviations

$\Delta\lambda_d$	Spectral line width as a result of Doppler broadening
ΔE	Photon energy
Δt	Transition lifetime
$\hbar$	Reduced Planck constant
λ_0	Center wavelength
ν	Frequency
ε_0	Permittivity of space
A	Einstein coefficient
C	Continuum intensity
E_n	Energy state
F	Force
h	Planck constant
M	Atomic mass
N	Energy state population
N_{rms}	Root mean square of noise
r	Distance
S	LIBS peak intensity
T	Temperature
t_d	Gate delay
t_g	Gate width
t_l	Laser-pulse width
AES	Atomic emission spectroscopy
CCD	Charged-coupled device
DDG	Digital delay generator
DP-LIBS	Double-pulse laser-induced breakdown spectroscopy

FWHM	full-width at half-maximum
ICCD	Intensified charged-coupled device
LIBS	Laser-induced breakdown spectroscopy
LIBS-LIF	Laser-induced breakdown spectroscopy laser-induced fluoresence
LOD	Lower limit of detection
LTB	Lasertechnik Berlin
MCP	Microchannel plate
ND-filter	Neutral density filter
Nd:YAG	Neodymium-doped yttrium aluminum garnet
NIST	National Insitute of Standards and Technology
OPO	Optical parametric oscillator
PDA	Photodiode array
RELIBS	Resonance-enhanced laser-induced breakdown spectroscopy
RMS	Root mean square
SNR	Signal-to-noise ratio

1 Introduction

Laser-induced breakdown spectroscopy (LIBS) is an atomic emission spectroscopy (AES) technique. It uses a high power pulsed laser in combination with a focusing lens to generate a plasma that ablates a small amount of matter from the surface of a sample. After an appropriate time delay, the plasma emission is collected and analyzed with a spectrometer. The photons emitted by the excited atoms and ions can give qualitative and quantitative information about the elemental composition of the sample.

LIBS was formulated only a few years after the development of the first laser in the 1960's. Between 1965 and 1995 less than 50 papers were published on LIBS each year. Since 1995 the interest in LIBS has risen dramatically, reaching more than 400 publications per year in 2004. Today, LIBS is often used by science and industry. A LIBS setup is used on the NASA rover "Curiosity", to determine the composition of rocks and soils on the surface of Mars [1].

Unlike conventional AES techniques (e.g. electrode spark and inductively coupled plasma) LIBS does not require physical contact with the sample. This makes remote analysis possible and makes sample preparation unnecessary [2, 3]. Even though LIBS ablates part of the sample (typically in the range of nanograms), LIBS is often considered non-destructive. LIBS has, however, one major drawback: the lower limit of detection (LOD) of LIBS is in the parts-per-million range, this not as good as other AES techniques, which typically reach parts-per-billion LOD's [4].

1.1 Enhanced LIBS

Several techniques exist to lower the LOD of LIBS. The most common techniques are double-pulse LIBS (DP-LIBS), where a second laser pulse is focused onto the plasma created by the first laser. The second laser creates an increase in ablated material and plasma volume, and a higher plasma temperature. Emission enhancements of up to 10-fold have been reported [5, 6].

A variation on the DP-LIBS combines LIBS with laser-induced fluorescence spectroscopy. In this method, often called LIBS-LIF , the second laser pulse is tuned to a specific transition wavelength of the element of interest. This second pulse enhances the fluorescence signal of the element and thus increases the signal-to-noise ratio [4]. Some cases are reported where the sensitivity is improved up to three orders of magnitude [7, 8]. A drawback of LIBS-LIF is that it cannot enhance the signal of multiple elements simultaneously.

Another approach overcomes this limitation and is related to both of the previous enhancements. The method is called resonance-enhanced LIBS (RELIBS) and has only recently been investigated. In RELIBS, the second laser pulse is tuned to a resonant transitional wavelength of an abundant element, instead of the trace element of interest as in LIBS-LIF. The energy absorbed by the abundant element is distributed over all elements through collisional transfers. Most of the RELIBS research has been done by the group of N.H. Cheung. LOD's of parts-per-billion were found [9–11].

1.2 Thesis outline

The goal during this internship was to build a RELIBS setup and investigate if it is a good method of enhancing LIBS. In this thesis the working and the results of a basic LIBS setup as well as RELIBS will be discussed. A LIBS setup was build and measurements of different samples are made and analysed using this setup. The LIBS setup is extended with a second laser to do RELIBS measurements on the same samples and compare the results. Chapter 2 contains some theory relevant to LIBS and RELIBS. In chapter 3, the layout and working of the experimental setup will be discussed in detail, as well as the procedures for the measurements. The results are shown and discussed in chapter 4. The final chapters give a conclusion and recommendations for further research.

2 | Theory

LIBS is an atomic emission spectroscopy technique. The high energy density from the focused laser pulse on the sample surface causes a plasma formation. In this chapter, the laser ablation and plasma emission is explained. The plasma emits radiation which consists of discrete lines, and bands and a continuum. The different types of radiation will be explained in section 2.2 and 2.3.

2.1 Laser ablation

When a laser pulse with enough power ($GW \cdot cm^{-2}$) is focused on the surface of a material, as result rapid local heating occurs. A small amount of material is vaporized, leaving a crater behind. Through further photon absorption the vapor is heated up until it is ionized and expands from the surface as a plasma plume.

Figure 2.1 shows several stages of the laser ablation. At different time intervals after the

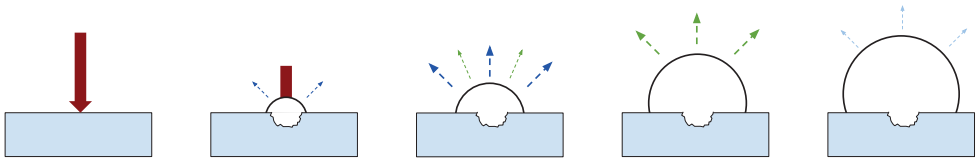

(a) Heating of target. (b) Free electrons. (c) Free electrons and atomic species. (d) Atomic species. (e) Molecular species.

Figure 2.1: Several stages of laser ablation and emission form the laser-induced plasma.

laser incidence, different radiations is emitted. In the early stages the radiation originates from free electrons. During the plasma expansion and cooling, spectral lines of atomic species are emitted. Later during plasma cooling, some molecular radiation is emitted. The plasma also creates a shock wave in the surrounding environment.

The interaction between the laser beam and the sample material is a complicated process and depends on many factors. Characteristics of the laser pulse such as the laser pulse duration and power fluctuations, is one of them. The chemical and physical characteristics of the material also influence the plasma. The ambient conditions are influential

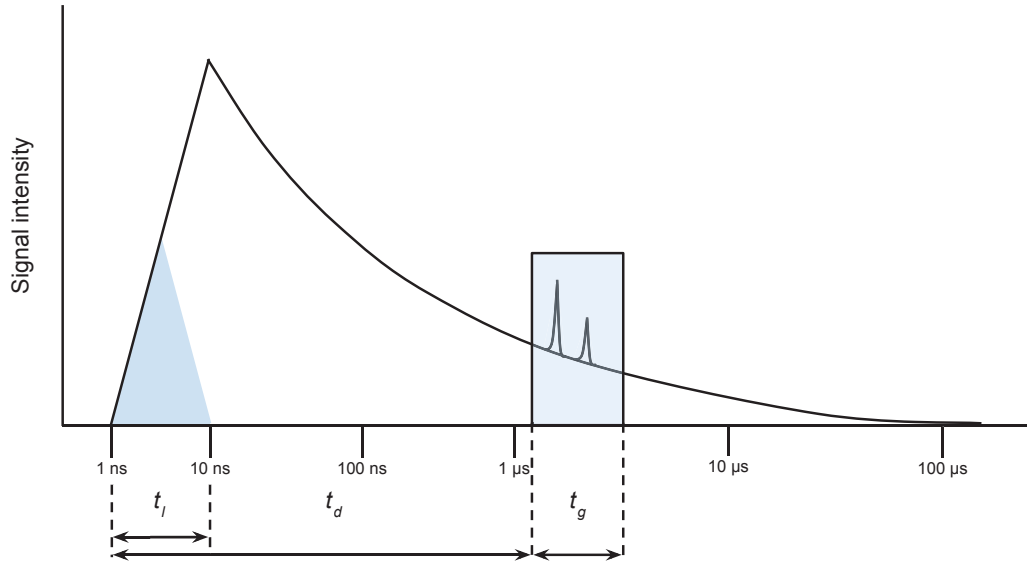

Figure 2.2: Laser-induced plasma evolution. t_l is the pulse width of the laser, t_d is the delay between ablation and the opening of the microchannel plate from the camera, and t_g is the acquisition window or gate width. Note that the time axis is in a logarithmic scale.

as well. All these factors make LIBS measurements difficult to reproduce, and therefore quantitative analysis is challenging.

2.2 Plasma emission

At the beginning of its lifetime the plasma emits a continuum of radiation. This continuum is a result of bremsstrahlung. Bremsstrahlung photons are produced when electrons collide with each other. The acceleration or deceleration due to collision results in the emission of a photon. The continuum holds no significant elemental information about the sample.

Figure 2.2 shows a schematic overview of how a laser-induced plasma evolves over time. Just after the laser pulse, the plasma emission increases and reaches its maximum on a nanosecond time scale. After this the plasma starts to cool down on a microsecond timescale. During the cooling down the excited electrons fall back to lower energy states and emit photons with a wavelength corresponding to the energy difference between the two energy states. In the the first microsecond, the continuum is dominant while only the strong spectral lines are visible. After a microsecond the continuum decreases enough for the spectral lines to be clearly visible. The continuum decays more quickly than the spectral lines, the lasting to several tens of microseconds. The intensity of the continuum is proportional to the temperature of the plasma.

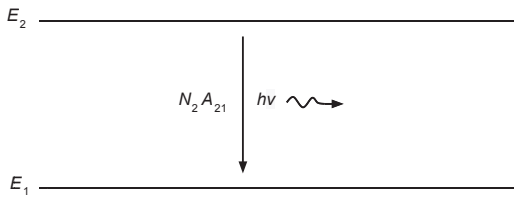

Figure 2.3: Spontaneous emission.

2.3 Spectral lines

The intensity of a observed spectral line depends on two factors: the intrinsic transition probability (and atomic population) and the conditions of excitation. The probability of an atom to spontaneously make a transition from energy state E_2 to E_1, is given by the Einstein coefficient A_{21}. The number of transitions is found by multiplying this coefficient with the population of E_2: N_2 (figure 2.3).

One of the excitation conditions that determines the line intensity is the opacity of the plasma. If a photon has no appreciable chance of being reabsorbed, the plasma is called optically thin. An optically thick plasma can re-absorb some radiation, decreasing the intensity of the spectral line.

2.3.1 Line broadening

The spectral lines from transitions in atomic spectra are never a single wavelength, but they always have a finite width. There are several sources that cause this broadening. In the ideal case only natural line broadening occurs. This broadening originates from the uncertainty in energy of the states that are involved in the transition (equation 2.1).

$$\Delta E \Delta t > \frac{\hbar}{2}, \tag{2.1}$$

where ΔE is the energy of the photon, Δt is the lifetime of the transition and $\hbar$ is the reduced Planck constant. Because of the short lifetime of an atomic energy state, the uncertainty in the measured energy is significant. This and the Fourier transform limit (because of the finite duration of a radiation process), give the spectral line its *natural line width*. In plasma spectroscopy however, this broadening is not significant because of other, more prominent, broadening effects. The typical natural line width at full-width at half-maximum (FWHM) is around 0.1 pm. The broadened line will have a Lorentzian profile.

Doppler broadening

Another cause of broadening is Doppler broadening. Because of the thermal motion, the spread of the atoms traveling towards the detector will differ from the spread of the rest

of the atoms by the Doppler shift. The resulting FWHM of the spectral line is given by equation 2.2.

$$\Delta\lambda_d = 7 \cdot 10^{-7}\lambda_0\sqrt{\frac{T}{M}}, \tag{2.2}$$

where $\Delta\lambda_d$ is the width as result of the optical Doppler effect, λ_0 is the center wavelength, T is the plasma temperature and M is atomic mass. Using equation 2.2 it can be found that a Lithium atom (M = 7 u) with a temperature of 10,000 K will have a Doppler broadening of 11 pm at a center wavelength of 413 nm. The broadened line will have a Gaussian profile.

Stark broadening

When the emitting atom is surrounded by dense plasma (as is the case for LIBS), both natural line and Doppler broadening are negligible in comparison with Stark broadening. Stark broadening is a result of the Stark effect. The Stark effect causes spectral lines of atoms to shift and split due to the presence of an electric field. The emitting atom interacts with the electric field of the charged particles around it. The force of the electric field at a distance r from the atom is given by equation 2.3.

$$F = \left(\frac{e}{4\pi\varepsilon_0 r^2}\right), \tag{2.3}$$

where ε_0 is the permittivity of space (F/m). When a hydrogen atom is considered, the perturbation of the energy levels, as a result of the electric field, is proportional to F. This results in a linear Stark effect. For all other atoms, the perturbation is proportional to F^2, giving a quadratic Stark effect. The linear Stark effect splits energy levels symmetrically, giving an unshifted broadened spectral line. As the quadratic Stark effect is proportional to F^2, the broadening is not symmetrical and the resulting broadened spectral line is also shifted. The shift of energy levels is larger for higher excitation energies, causing the transition frequencies to be reduced. Thus, the shift occurs towards longer wavelengths.

A typical FWHM from Stark broadening, for a plasma temperature of 10,000 K and an electron density of 10^{17} cm^{-3} is 0.68 nm for a lithium line at 413.2 nm [2].

2.4 Signal enhancement

One drawback of LIBS is its relatively poor detection sensitivity compared to other, conventional, analysis techniques. The LOD depends on the element, but is usually in the parts-per-million range for solids. To increase the LOD, further excitation of the plasma species is required.

2.4.1 Double-pulse LIBS

Double-pulse LIBS is often an used method to enhance the LIBS signal. Double-pulse LIBS uses one laser pulse to ablate the sample and after a delay a second pulse intercepts

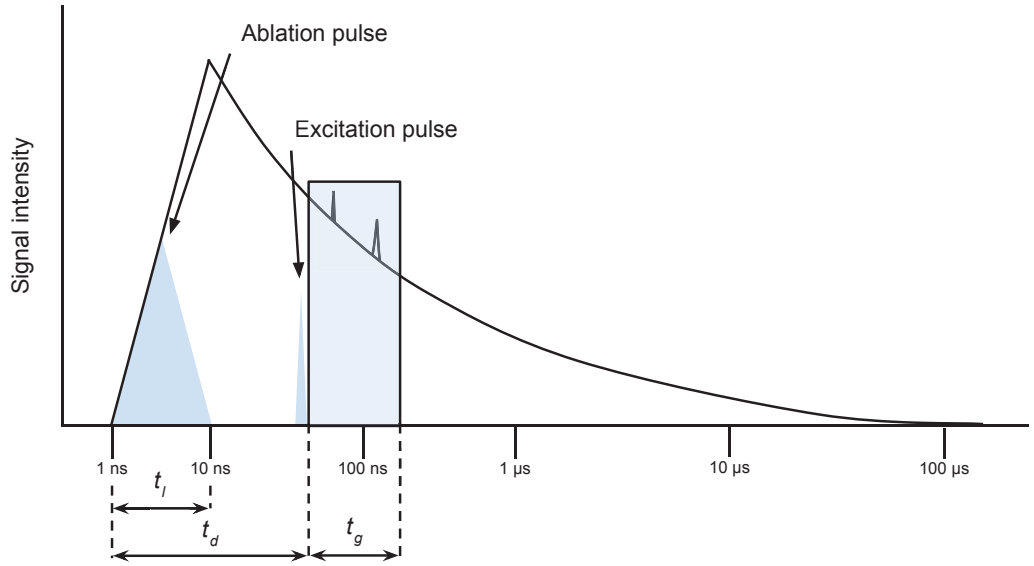

Figure 2.4: Resonance-enhanced laser-induced plasma evolution.

the plasma. The delay between the two lasers is usually in the order of microseconds. The advantages can clearly be seen when comparing double-pulse with single-pulse LIBS [12]. Even when the total laser irradiance is the same in both cases, enhancements are clearly visible [6]. Several enhancement effects are: increased sensitivity, line emission narrowing, enhancement of ablation efficiency and improved signal reproducibility. The reason for these enhancements, however, is not fully understood. Some hypotheses on how double-pulse LIBS enhancements could occur are: direct energetic coupling between two plasmas and sample heating by the first plasma resulting in more ablation and a higher temperature with the second plasma [12].

2.4.2 Resonance-enhanced LIBS

A variation on double-pulse LIBS is resonance-enhanced LIBS or RELIBS and can potentially enhance the LIBS signal even further. With resonance-enhanced LIBS the second laser pulse is tuned to a specific wavelength rather than an arbitrary one as with the double-pulse method. The wavelength is tuned to a resonant energy transition from an abundant element in the sample material. This causes a photoionization instead of a thermal ionization, making more efficient use of the laser energy. Figure 2.4 shows the evolution of the laser-induced plasma for RELIBS. As depicted in the figure, the delay between the two lasers is in the order of tens of nanoseconds, rather than microseconds as with double-pulse LIBS.

When the excitation laser intercepts the plasma plume and photoionizes the abundant element, this element can distribute the absorbed energy to other elements present in the plasma. This increases the signal not only from the selected element, but potentially also from other present elements including trace elements that were previously barely or not visible. The full mechanism of this process is not yet fully understood, but the

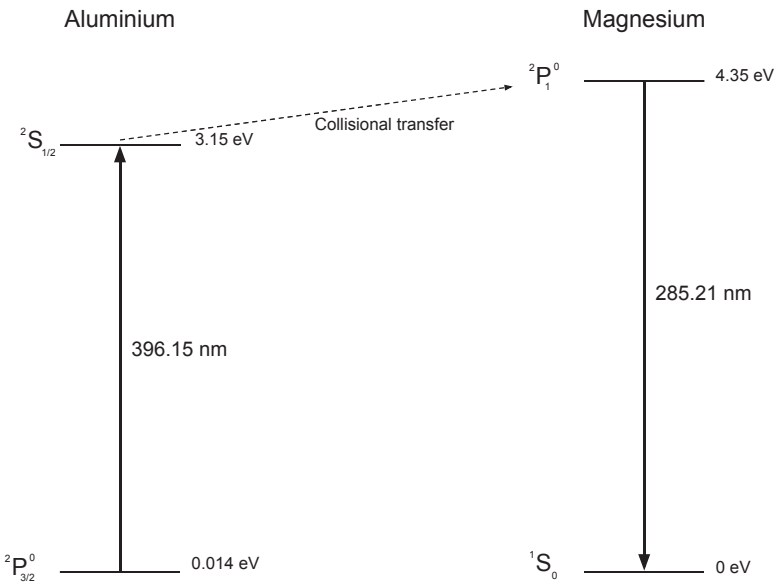

Figure 2.5: Partial Grotrian diagram for excitation of magnesium from selective excitation of aluminum [13].

energy transfer happens most likely through particle-particle collisions. An illustration of this energy transfer in an aluminum alloy is shown in figure 2.5 in a partial Grotrian diagram.

The effects of resonant-enhanced LIBS are most prominent when low ablation energies are used, preferably near the ablation threshold. The resonant-enhanced LIBS enhancement diminishes when more of the sample is destroyed. This is a result of a faster plume expansion at higher ablation energies [14].

3 | Experimental setup

Figure 3.1 shows the setup for regular LIBS experiments. The used ablation laser is a nanosecond pulsed Nd:YAG laser (specification of the laser are listed in section 3.1). The light from the ablation laser is reflected towards the breadboard with a dielectric coated mirror. This mirror has a high damage threshold and is optimized for a high reflectivity of 1064 nm light. After the first mirror, the light goes through a neutral density filter (ND-filter) to attenuate the light. This filter is removed for some measurements. After the ND-filter, the light is reflected with a second and a third mirror, down onto the sample. Figure 3.2 shows two side views of the area enclosed by the dotted line in figure 3.1. The light passes through a bi-convex lens with a focal length of 50 mm. Using a vertical stage, the surface of the sample is positioned in the focal point of the lens, where the plasma will be formed. The LIBS signal is captured onto a fiber-optic cable by the collection optics. The fiber-optic cable is connected to the echelle spectrometer with an ICCD camera attached to it (the spectrometer and camera are discussed in more detail in section 3.2). To ensure the proper timing between the firing of the laser pulses and the acquisition of the camera, both the camera and the laser are connected to a digital delay generator (section 3.3).

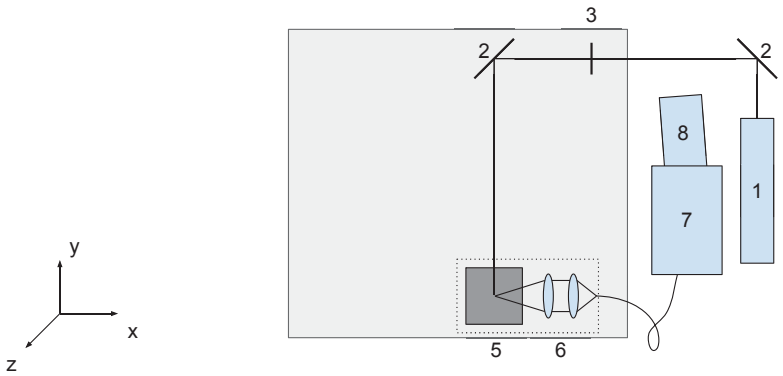

Figure 3.1: Top view of the LIBS setup on top of a breadboard (gray area). 1: ablation laser, 2: dielectric mirror, 3: ND-filter, 5: sample, 6: collection optics, 4: spectrometer, 8: camera.

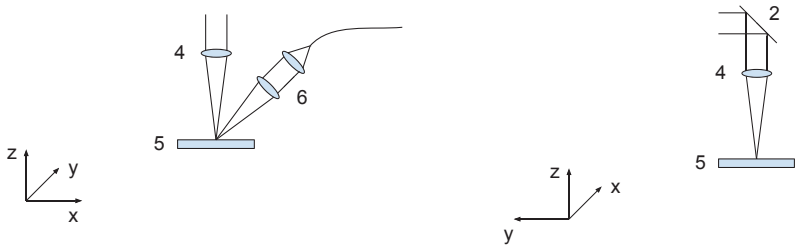

Figure 3.2: Side views of LIBS setup. 2: downwards directing dielectric mirror, 4: focusing lens.

The layout of the LIBS setup was chosen with a future upgrade to resonance-enhanced LIBS in mind. For the RELIBS setup, a second laser is added to setup as depicted in figure 3.3. This is the excitation laser and fires a pulse with a delay relative to the pulse from the ablation laser. The light from the excitation laser is reflected towards the breadboard with two aluminum mirrors. On the breadboard the beam is lowered and directed towards the sample using a periscope. Using a lens and a down facing mirror, the light is focused on the sample surface and overlapped with the ablation laser. The periscope and focusing optics are shown in more detail in figure 3.4.

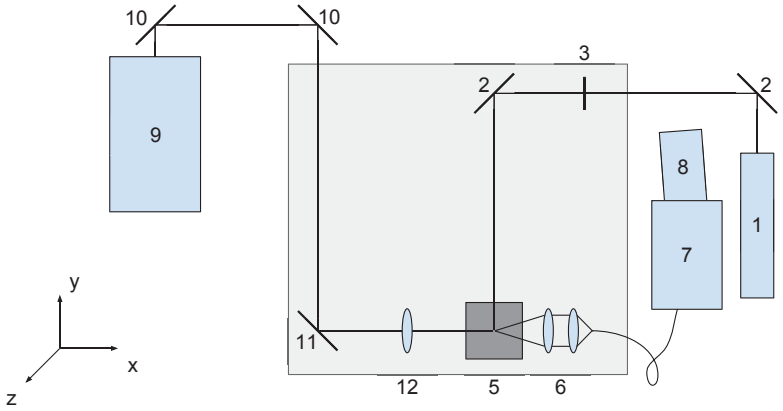

Figure 3.3: Top view of the RELIBS setup. 9: excitation laser, 10: aluminum mirror, 11: periscope, 12: focusing lens.

The sample is placed on a motorized translation stage (14 in figure 3.4) that moves the sample horizontally in one dimension. This stage is moved after each measurement so that a fresh spot is ablated by every laser pulse. The stage is a Newport MFA-CC and is controlled by a Newport ESP300 motion controller.

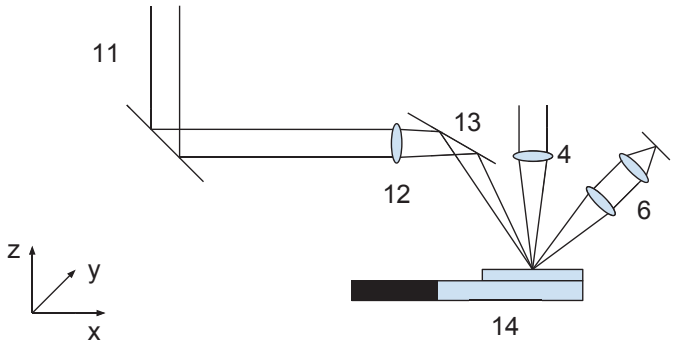

Figure 3.4: Side view of the RELIBS setup. 13: downwards directing aluminum mirror, 14: translation stage.

3.1 Lasers

Ablation laser

The laser used for the sample ablation is a Q-switched Nd:YAG laser from the Brilliant series of Quantel. The Brilliant is Q-switched Nd:YAG laser with a repetition rate of 20 Hz. It is pumped by a flash lamp and has a specified maximum output energy of 360 mJ. The output energy was measured, however, to be 340 $\pm$ 3 mJ. The pulses have a duration of 5 ns at FWHM. The output light has a wavelength of 1064 nm. The beam profile was checked with a piece of ablation-paper and is depicted in figure 3.5. With the ND-filter in place, the beam profile could not be determined because the energy was attenuated below the ablation threshold of the paper.

Figure 3.5: Beam profiles of the ablation laser. From left to right: at a distance of 0 m from the laser; after the first mirror, at a distance of 0.1 m; at the position of the ND-filter, a distance of 0.6 m from the laser.

The power supply and cooling are situated in an external cabinet on wheels. The connectors for external triggering and the remote control box are on the cabinet as well. The laser head is connected to the cabinet with an umbilical cable. Specifications and quality control from the manufacturer can be found in appendix A. The Brilliant functions are controlled with a remote control box. The triggering of the laser is controlled by an

external digital delay generator. The flash lamp is triggered first and after a delay of 200 μs the Q-switch is triggered. This is the optimum delay for a high energy and stable output. By changing this delay the output energy of the laser can be tuned. However, changing this delay decreased the accuracy of synchronization with the excitation laser and camera. The delay was therefore kept at the optimum and the output energy was attenuated with a ND-filter as shown in figure 3.3.

Excitation laser

The excitation laser is a pulsed solid state tunable laser from Ekspla (NT242-SH). The laser consists of a diode-pumped Q-switched Nd:YAG laser and an optical parametric oscillator (OPO). The pulse duration is 7 ns and the laser has a repetition rate of 1000 Hz. The output energy depends on the selected wavelength, figure 3.6 shows the pulse energy as a function of wavelength. The different colors stand for the different output beams that are selected within the OPO. Unlike the ablation laser, this laser cannot be externally

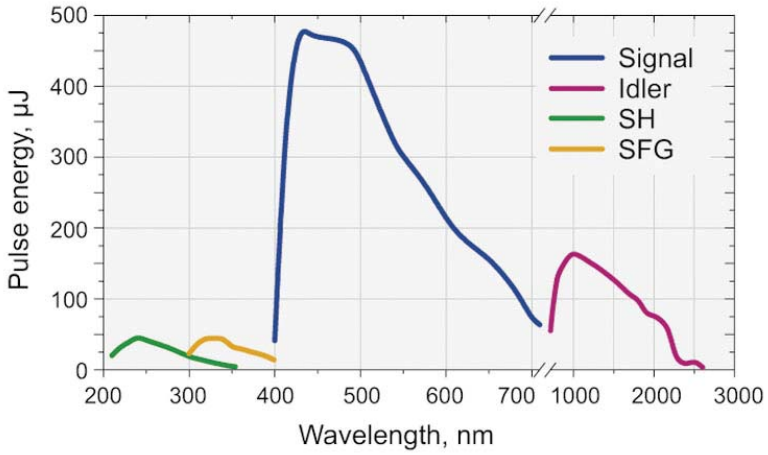

Figure 3.6: Energy output of the excitation laser as a function of wavelength. SH: second harmonic, SFG: sum frequency generation.

triggered or fire a single pulse. It does however, have a synchronization output signal synchronized with the laser pulses. This signal is used to synchronize the laser to the rest of the setup. Appendix B shows more detailed specifications as well as the beam profile of the laser.

3.2 Spectrometer and camera

The spectrometer used in this setup is an ARYELLE 200 from Lasertechnik Berlin (LTB) . Attached to the spectrometer is an Andor iStar Intensified CCD camera. Specifications for the camera and spectrometer can be found in appendix G and F respectively. The spectrometer has a custom modification for a fiber optic cable connection.

3.2.1 Echelle spectrometer

The used spectrometer is an echelle spectrometer. Conventional spectrometers use diffraction gratings to disperse the light. The spectrum is then recorded at the focal plane on a photodiode array (PDA) or CCD. The spectral range in such a setup is limited by the width of the focal plane and PDA or CCD. An echelle spectrometer makes use of the two-dimensional capabilities of a CCD.

The working of a simple echelle spectrometer is depicted in figure 3.7. The echelle spec-

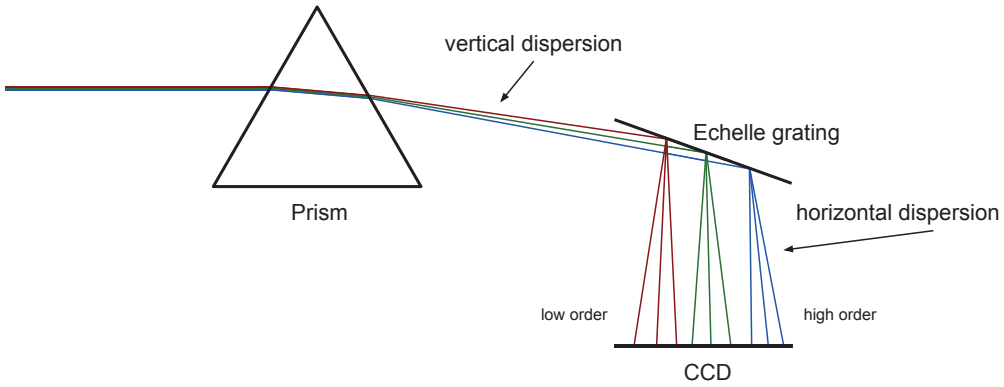

Figure 3.7: Basic working of an echelle spectrometer.

trometer makes use of cross-dispersion. Light from the entrance slit of the spectrometer is dispersed first by a prism. After the prism, a perpendicular positioned echelle grating separates the light into many diffraction orders, each order containing a part of the spectrum, with some overlap. This configuration leads to an output where the orders are stacked upon each other, forming an echellogram (figure 3.8). Figure 3.8a shows the spectrum of a continuous light source and figure 3.8b of a light source with some spectral lines in addition to some continuum. Note that a continuous light source generates uninterrupted lines, while spectral lines generate individual dots. This is well suited for a two-dimensional CCD and makes a high resolution ($\sim$0.1 nm - 0.5 nm) spectrometer in a relative compact housing possible. An echelle grating is different from other gratings. It has fewer lines grooves per millimeter than a regular grating and has a higher blaze angle.

3.2.2 Intensified CCD Camera

Attached to the spectrometer is an ICCD camera. This is the detector of choice for LIBS measurements, because it provides time-gated detection in the order of microseconds or even nanoseconds. This is not possible with mechanical shutters.

An ICCD camera is a CCD camera with a microchannel plate (MCP) attached to it. An MCP is a thin sheet of glass tubes parallel to each other forming a disc like shape. The glass tubes are around 10 μm in diameter and a typical MCP contains between 10^4 and 10^7 tubes. Figure 3.9 shows a diagram of an ICCD containing an MCP.

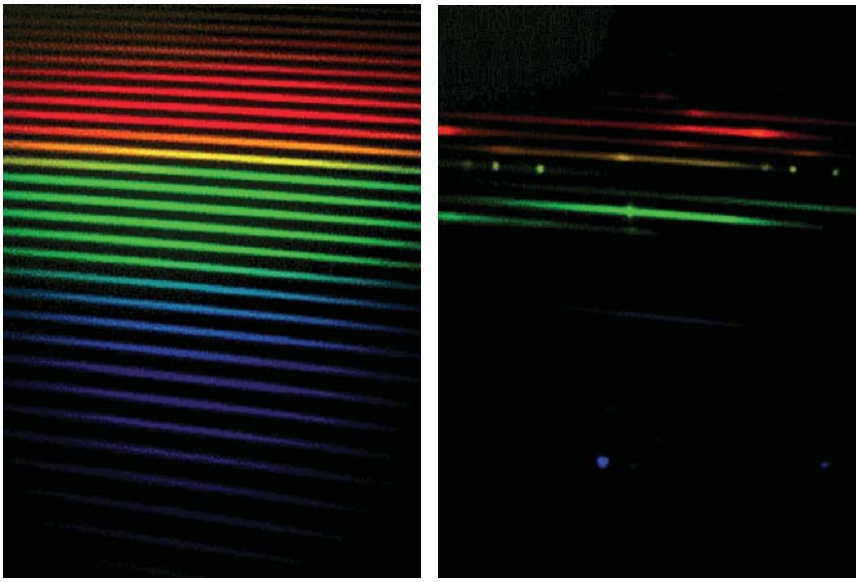

(a) Spectrum of a tungsten lamp. (b) Visible spectrum of a fluorescent lamp.

Figure 3.8: Echellograms of different light sources.

With a voltage applied between the front and back of the device the gate is open. When a photon hits the photo cathode, an electron is liberated and travels to the other end of the MCP. When the electron hits the luminescent phosphor screen at the other side of the MCP, a photon is produced and moves to the CCD through the fiber optic coupling. When there is no applied voltage, no electrons travel along the tubes and the gate is effectively closed. Because of the acceleration of the electron by the applied voltage, it can free more electrons as it travels. By adjusting the voltage a single photon can give rise to as many as 10^3 electrons. This gain is not used in the measurements presented in this thesis.

The resulting image on the CCD is readout with software supplied by the manufacturer (Sophi). Sophi converts the echellogram to a wavelength dependent spectrum. As can be seen in figure 3.8a, the intensity of the spectrum from the echellogram decreases towards the edges. To compensate for this, a intensity standardization is performed with a calibrated halogen lamp. The wavelengths are calibrated using a mercury-argon lamp. Sophi also controls the acquisition time and the cooling of the CCD. The CCD is cooled to -30° Celsius to minimize thermal noise. Other controls, like the gating of the MCP and the start of acquisition are controlled by the DDG (section 3.3).

3.3 Digital synchronization

As mentioned in chapter 2 the light emitting from the plasma changes over time. The continuum is dominant in the early stages of the plasma and decays after some time, making the LIBS peaks visible. The exact nature of this process differs per sample, therefore, the timing must be adjustable. To control the timing between the ablation

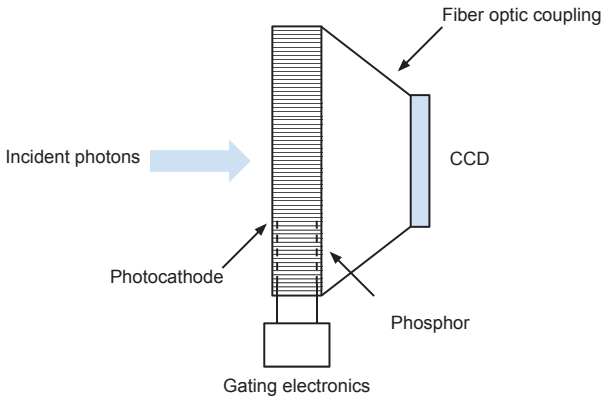

Figure 3.9: Diagram of a typical ICCD setup.

laser and the camera, a digital delay generator (DDG) is used (Highland T564). It offers four programmable pulse output channels. Delays and widths of the pulses can be varied between 0 s and 10 s with a resolution of 10 ps, for each channel separately (see appendix C for more specifications).

LIBS

For the LIBS measurements, four channels of the DDG are used. Channel A is connected to the flash lamp of the ablation laser, channel D to the Q-switch of the ablation laser, channel B to the direct gate input and channel C to the trigger of the ICCD camera. An overview is shown in figure 3.10. After it receives a trigger signal from the computer, the DDG is programmed to send a pulse signal through all channels, with the specified delays. Figure 3.11 shows the scheme of the time delays and pulse widths for the different signals. The first signal is sent to the external flash lamp trigger. After a delay of 200 μs, a signal is send to the external Q-switch trigger and a laser pulse is fired. After a delay of a few microseconds a signal to the camera's external trigger is send. On the rising edge of the signal the CCD starts acquisition. The acquisition time is defined in the software and is not controlled by the external trigger, thus the falling edge of the signal is ignored. 5 μs after the rising edge of the signal for the camera trigger, a signal is send to the camera's direct gate input. From this time on, the signal from the plasma is measured with the CCD. In contrast to the signal for the trigger, the signal for the direct gate input does control the width of the gate. The width of the gate varies between 1 μs and 100 μs, depending on the measurement.

Resonance-enhanced LIBS

For the resonance-enhanced LIBS setup, the excitation laser must be synchronized with the ablation laser. Because of the lack of a working external trigger for the excitation laser, this laser is left constantly running and its output synchronization signal is used as a trigger for ablation laser and camera (master trigger). This output signal is connected to

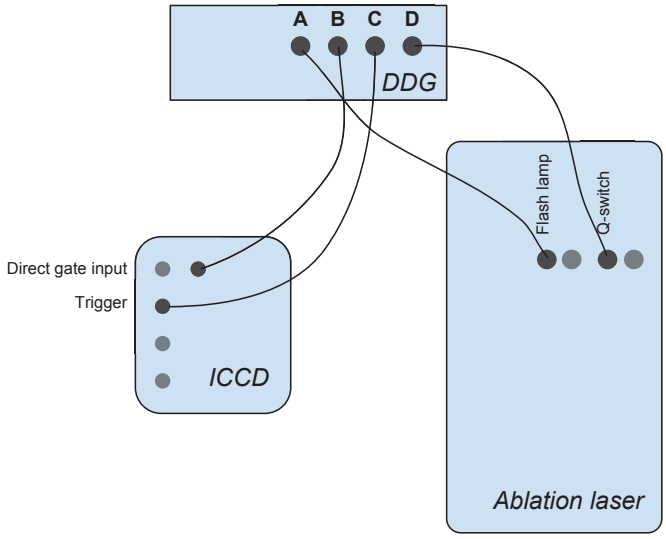

Figure 3.10: Connectivity of the digital delay generator.

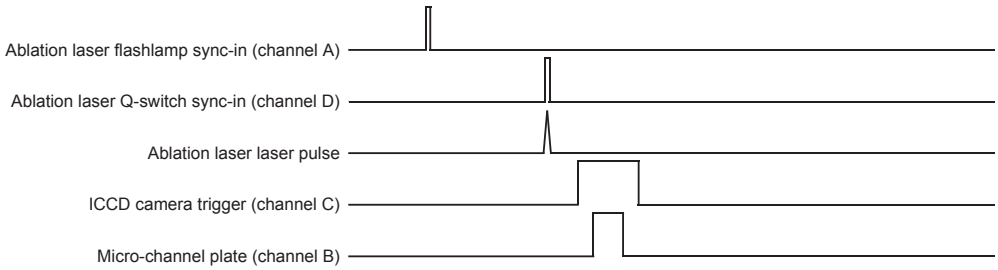

Figure 3.11: LIBS timing overview.

the external trigger input of the DDG and the output channels A-D are triggered with the appropriate delays. Figure 3.12 shows the timing scheme of the RELIBS synchronization. The bottom five signals are the same as for the LIBS scheme (figure 3.11), the top two signals are the additions for the excitation laser. The master trigger (excitation laser sync-out) is used to trigger the DDG on the rising edge of the signal. From this moment on the DDG starts the delays for all four output channels. The falling edge of the master trigger fires the actual laser pulse from the excitation laser. The delay between the master trigger and the ablation laser pulse is set such that the ablation laser pulse is fired before the excitation laser pulse, with a delay between 0 and several hundreds of nanoseconds.

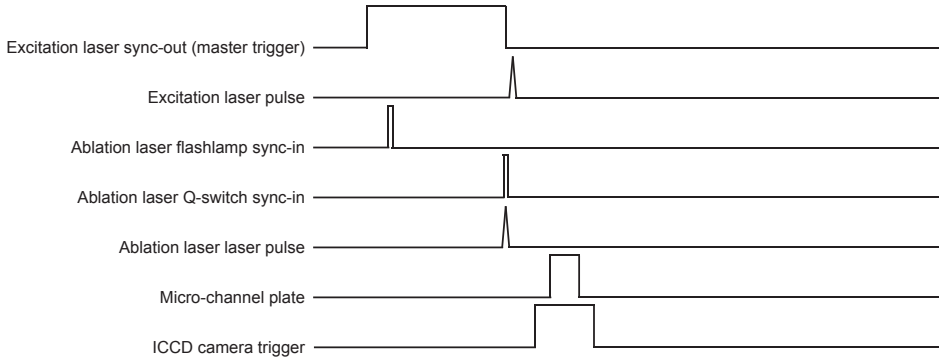

Figure 3.12: RELIBS timing overview.

The problem of different repetition rates of the two lasers (1000 Hz for the excitation and 20 Hz for the ablation laser) is solved in the DDG. A function called burst logic is used for this purpose. With burst logic two variables are defined: N and M. When triggered the DDG fires N output pulses for every M triggers. In this setup $N = 1$ and $M = 50$. The DDG is controlled through a RS323 interface, which is connected to a computer. From the computer the delay and duration of the different output channels are specified, using a Matlab script. For this setup a custom function is written to correctly configure the DDG. This function is shown in appendix E and provided with comments.

Every measurement is performed with the use of a computer. The DDG, the motion controller for the translation stage and the spectrometer are all connected to this computer. Prior to a measurement, Sophi is setup to acquire and save the measured spectra. All measurements are performed from Matlab. A custom script was written for Matlab to configure and control the DDG and to control the translation stage. With this script multiple measurements in different spots can be performed automatically. The source code of the Matlab script can be found in appendix D. After a series of measurements is performed, the spectra are loaded in Matlab for analysis.

To ensure that the timings between the two lasers and the camera are correct, an oscilloscope and two photodiodes are used to check the timings. A silicon photodiode was used for the excitation laser and a germanium photodiode for the ablation laser. The oscilloscope has a bandwidth of 500 MHz and four channels. To avoid damaging the photodiodes with the high energy laser pulses, the laser pulses are reflected from a piece of paper or metal. Figure 3.13a shows a screenshot of the oscilloscope when looking at the two laser signals and the signals for the camera, every division stands for 50 μs. Figure 3.13b shows a more detailed picture of the timing between the two lasers and the camera gate, every division here stands for 50 ns. The double lines are a result of jitter. Also in figure 3.13b channel 2 shows a small bump in the rising edge, this is most likely some scattered reflection of the ablation laser.

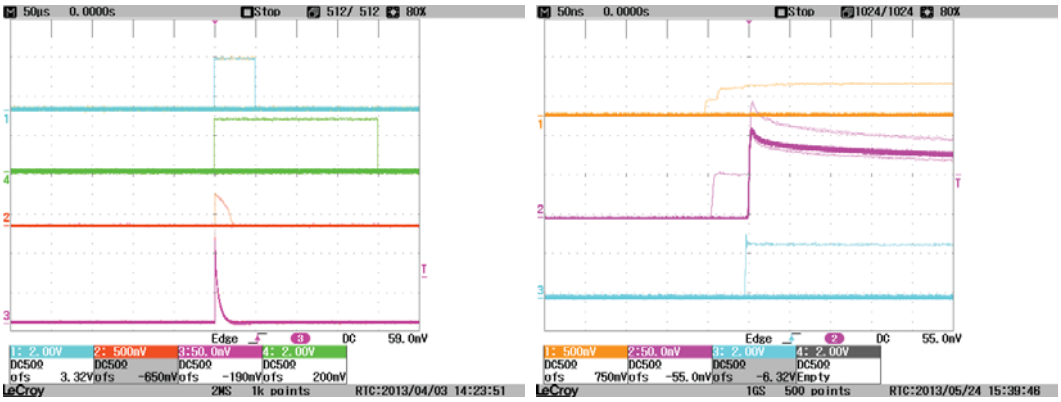

(a) Channel 1: direct gate input, channel 2: ablation laser, channel 3: excitation laser, channel 4: camera trigger, 50 μs per division.

(b) Channel 1: ablation laser, channel 2: excitation laser, channel 3: , channel 4: direct gate input, 50 ns per division.

Figure 3.13: Screenshots of oscilloscope readings.

4 Results and discussion

This chapter is divided into two main sections: regular LIBS and resonance-enhanced LIBS. The regular LIBS measurements have been done to get a general idea of LIBS and to serve as a reverence to quantify the improvement a RELIBS provides. To overcome the problem of poor reproducibility, the spectra for comparing LIBS and RELIBS are averages of at least 25 laser pulses. Between every laser pulse the sample was moved horizontally by the translation stage, to expose an undamaged area on the sample surface for each pulse. The peaks that are identified in the obtained spectra are compared with values from the National Institute of Standards and Technology's (NIST) electronic database [15].

4.1 LIBS

To be able to get the best signal-to-noise ratio (SNR) from a LIBS measurement, knowledge on how the plasma evolves over time is experimentally obtained. Because basalt gives a large LIBS signal and has many peaks over a broad spectrum, it is used for the experiment on plasma evolution. Measurements are taken at different time intervals or gate delays (t_d) ranging from 0 μs to 4.45 μs with a constant gate width (t_g) of 1 μs. A short gate width is desired for a good time resolution, however a short gate width also means little light reaching the CCD. To increase the amount of light, 10 pulses were fired for every measurement. These pulses were fired with the repetition rate of the ablation laser (20 Hz). The gate (MCP) was opened and closed for every pulse, so that the gate opened and closed 10 times per measurement. The CCD acquisition time was 1500 ms, meaning that every spectrum has the signal of 10 pulses added together.

The spectra from the measurements are plotted as a function of time in figure 4.1. A better overview of the continuum intensity and LIBS intensity over time is given in figure 4.2. For the continuum intensity, the average number of counts in the spectral region of 525 nm to 550 nm is taken. For the LIBS intensity, the number of counts for the Fe I peak at 396.93 nm is plotted. Judging from these figures, the best SNR can be achieved with a gate delay between 1 μs and 1.5 μs and a gate width of at least 3 μs.

On first look it seems that the LIBS peaks start at around $t_d = 0.40$ μs. However, because of the 1 μs gate width, the spectrum acquired at $t_d = 0.40$ μs also contains signal from $t_d = 0.4$ μs until $t_d = 1.40$ μs. Because there are no LIBS peaks before 0.40 μs the LIBS peaks seem to start just before 1.40 μs after ablation. This is where LIBS peaks would be expected. At this point the continuum is already less intense, indicating that the

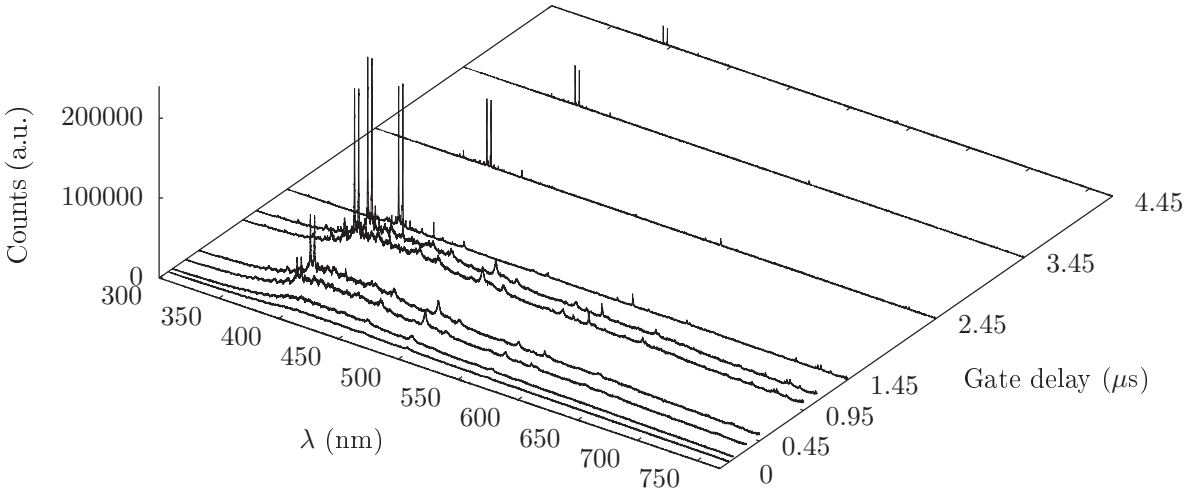

Figure 4.1: Basalt spectrum evolution over time. Gate width $t_g = 1$ μs, 10 pulses per measurement.

plasma is cooling down and ions fall back to their lower energy states.

Element identification

With the optimum gate delay and gate width determined, measurements can be taken to identify elements by comparing their peaks with literature values. The composition of the basalt sample was known beforehand and is shown in table 4.1.

Table 4.1: Elemental composition of basalt sample.

Element	Mass proportion [%]
O	45.80
Si	22.40
Fe	9.16
Al	8.47
Ca	6.20
Mg	3.71
Na	2.56
Ti	1.43
K	0.79
Sr	0.035
Ba	0.038

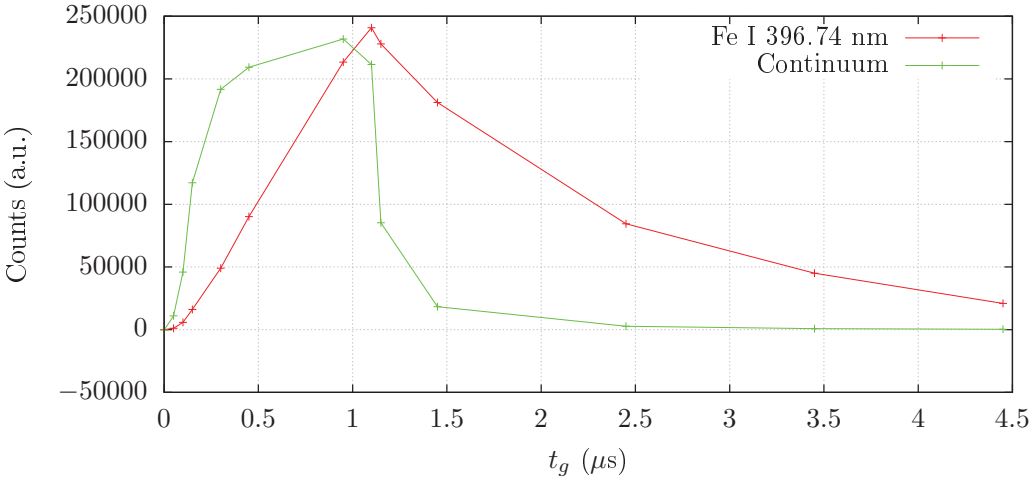

Figure 4.2: Averaged intensity for the continuum and Fe I peak as a function of time

Since the main goal of this thesis is to determine if RELIBS is a good enhancement for LIBS, the identification of elements was limited to only the most prominent peaks. Figure 4.3 shows the spectrum of basalt for a $t_d = 1.30$ μs and $t_g = 100$ μs. One pulse was fired at full laser power. The peaks identified from the spectrum are shown in table 4.2. The relative intensity of most of the peaks from figure 4.3 correspond roughly with what is expected from looking at the composition of the sample.

Table 4.2: Identified ions from basalt measurement.

Ion	Observed wavelength [nm]
Si I	390.55
Ca II	393.36
Fe II	396.79
Ti I	399.86
Ca I	422.65
Ca I	445.48
Mg I	516.73
Mg I	517.27
Mg I	518.36
Ca I	558.88
Ca I	589.00
Si II	634.71

Oxygen and silicon, however, deviate. Silicon has very weak peaks and oxygen shows no peaks at all. In the case of silicon, this can be explained by the fact that it's strong peaks are mainly in the ultraviolet, between 200 nm and 300 nm. Some peaks are in the visible spectrum, but they are relatively weak. Oxygen is known for it's poor detectability with LIBS [16], which is the main reason for it's absence in the basalt spectrum. The strongest peaks of oxygen are also out of the range of the spectrometer, as they are in the extreme ultraviolet.

Oxygen is not the only element that is poorly detectable with LIBS. All elements have

a different sensitivity for LIBS [16]. The reason for this variance is quit complex and is not a part of this thesis. Aluminum is another element present in basalt that is found from the LIBS spectrum. There are aluminum peaks visible, the ion Al I at 396.15 nm for example.

A titanium alloy sample was also measured. Unlike the basalt, the composition of the titanium alloy is unknown. Figure 4.4 shows its LIBS spectrum. This spectrum is an average of 50 measurements and will be compared to a RELIBS measurement in the next section. In order to be able to make a fair comparison with that particular RELIBS spectrum, the gate delay and the gate width are set to the same values. Also, the energy of the laser is attenuated (see section 4.2). The gate delay is set to 50 ns, the gate width t_g is 30 μs and one pulse per measurement was used. The exact pulse energy was not measured because the high energy would damage any available power sensors. Because the spectrum is averaged over 50 measurements, most of the energy fluctuations of the laser will be insignificant.

The main peaks that are identified from the LIBS spectrum, are originating from titanium. From the spectral line identification, it is clear that the alloy also contains some aluminum, other elements have not been found. As can be seen in figure 4.4, titanium has a lot of peaks of it's own and is very suitable for LIBS. A selection of identified peaks is shown in table 4.3. The amount of continuum is relatively low, this is most likely due to the low ablation energy. This gives a relatively cool plasma resulting in little continuum.

Table 4.3: Identified ions from titanium alloy spectrum.

Ion	Observed wavelength [nm]
Ti II	376.13
Al II	396.15
Ti II	416.38
Ti II	430.00
Ti I	453.40

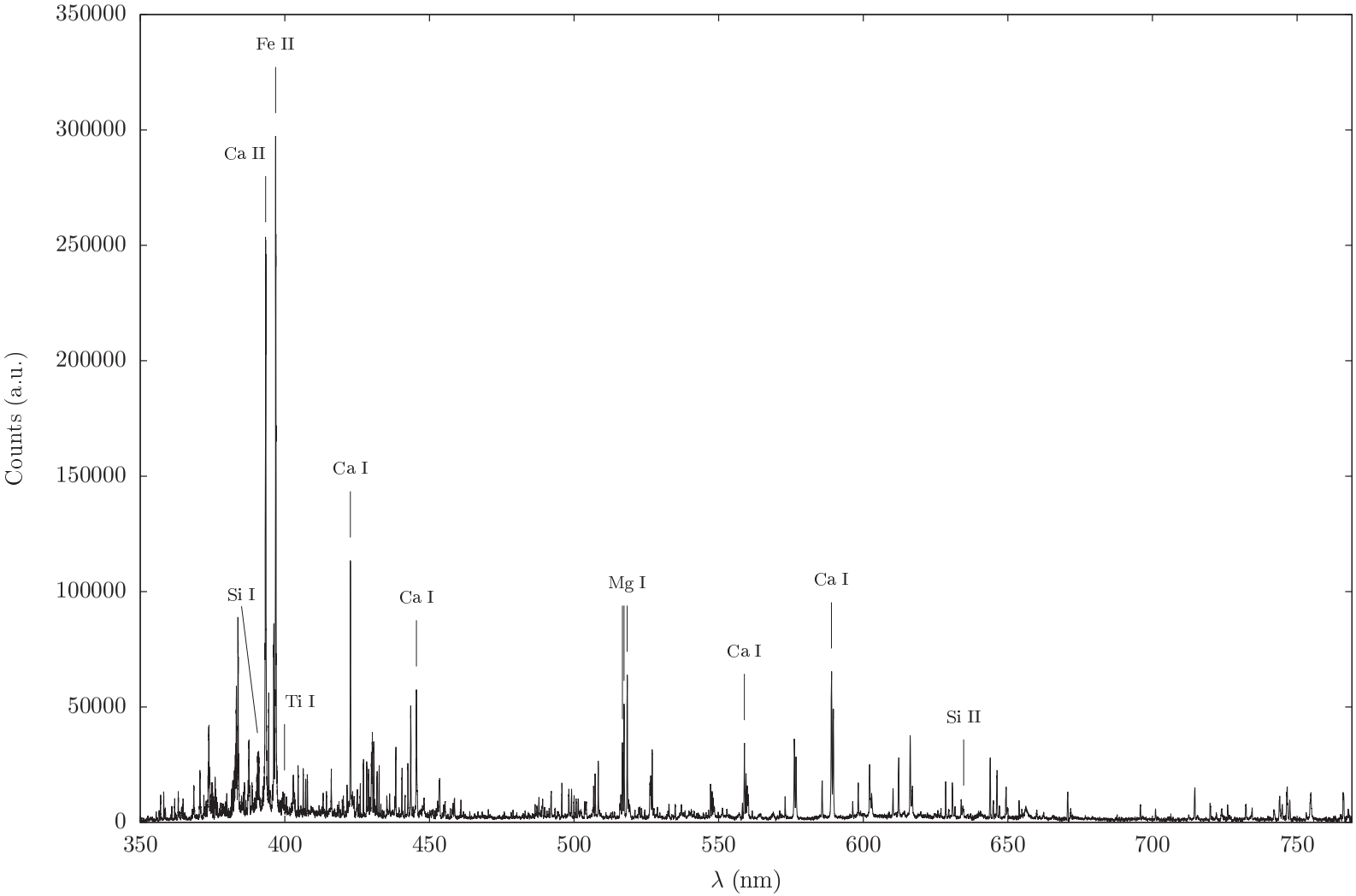

Figure 4.3: LIBS spectrum of basalt.

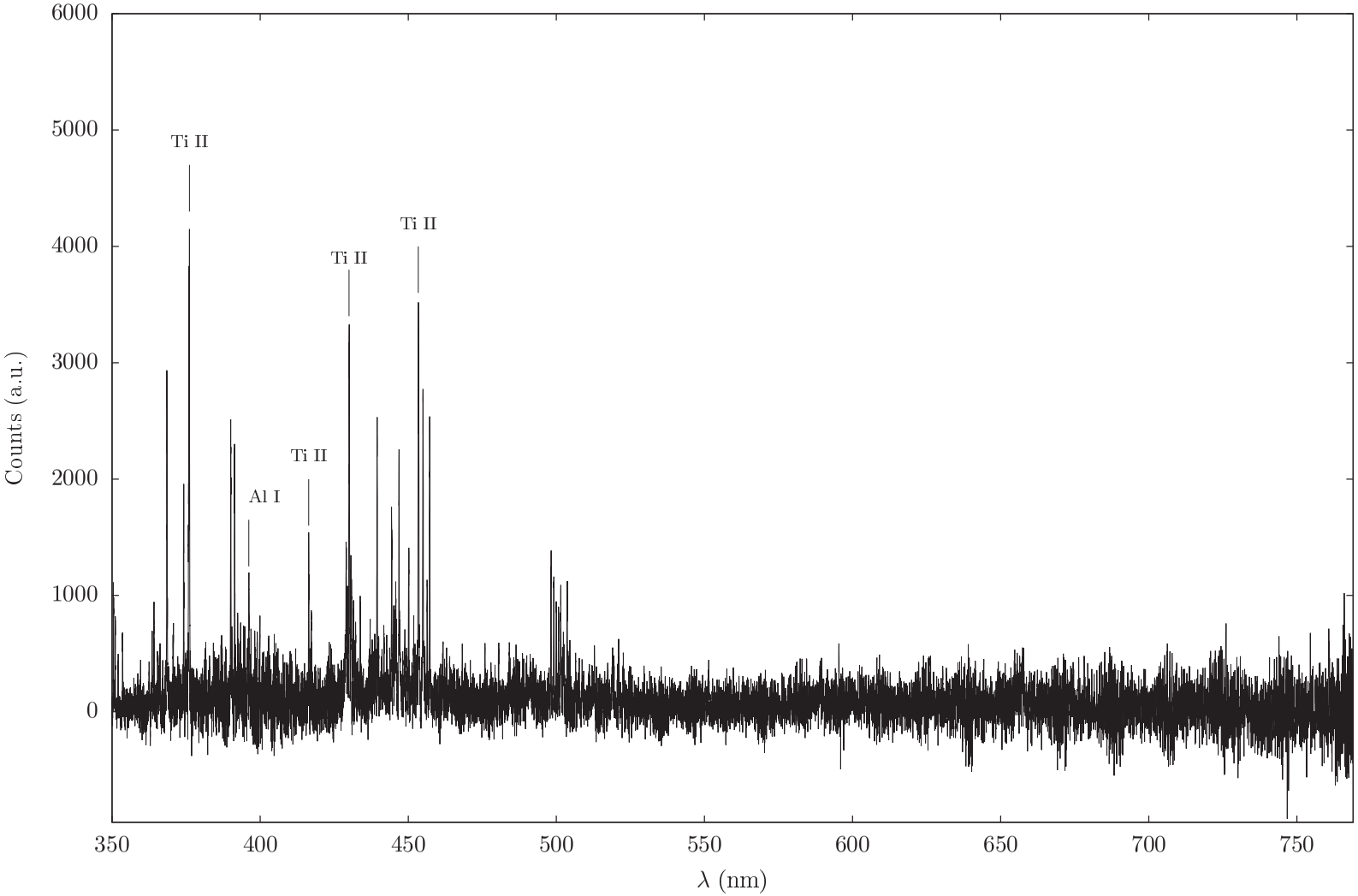

Figure 4.4: LIBS spectrum of titanium alloy.

4.2 Resonance-enhanced LIBS

Resonance-enhanced LIBS measurements are performed on a steel alloy and a titanium alloy. The samples are small flat slabs. These measurements were compared with single-pulse LIBS measurements on the same sample. The samples chosen for the RELIBS measurements are chosen for their resonant photoionization wavelengths. This setup is limited to elements with resonant photoionization wavelengths between 400 nm and 500 nm, because the excitation laser has enough energy only in this region (see figure 3.6).

Titanium alloy

A titanium alloy was chosen because titanium works well with LIBS and it has photoionization wavelengths within the available region. The wavelength used to excite the titanium is 496.73 nm [17]. The resonance-enhanced LIBS spectrum of the titanium alloy is compared to a single-pulse LIBS spectrum in figure 4.7. Measurements were carried out with the full power of the ablation laser. The beam from the excitation laser was not focused directly on the sample surface, instead the surface was just outside the focal point to prevent a second ablation. When comparing the two spectra it is clearly visible that most of the peaks in the resonance-enhanced LIBS spectrum are stronger.

For comparison with the regular LIBS spectrum, the SNR of several peaks is determined in both spectra and compared. The SNR is determined by dividing the intensity of the peak by the noise of a nearby region of continuum (see equation 4.1 and 4.2).

$$\mathrm{SNR} = \frac{S - C}{N_{\mathrm{rms}} - C}, \tag{4.1}$$

where S is the intensity of the peak, C the intensity of the continuum and N_{rms} the RMS of the region with noise.

$$N_{\mathrm{rms}} = \sqrt{\frac{1}{n}\left(N_1^2 + N_2^2 + \cdots + N_n^2\right)}. \tag{4.2}$$

The noise is determined by taking the root mean square (RMS) of the intensity of the continuum region. The intensity of the continuum is then subtracted from the LIBS peak and the noise to exclude the influence of a potential risen continuum.

For example: in the case of the aluminum peak at 396.15 nm in the titanium alloy the region from 383.11 nm to 386.50 nm was used for the noise calculation. Table 4.4 compares the LIBS SNR and RELIBS SNR of an Al I peak and a Ti II. The enhancement

Table 4.4: SNR ratio's of ions from titanium alloy spectrum.

Ion	Observed wavelength [nm]	LIBS SNR	RELIBS SNR
Al I	396.15	22	127
Ti II	453.40	112	777

for the Al I at 396.15 nm is almost 6-fold, while the enhancement for the Ti II at 453.40 nm is almost 7-fold.

To investigate if the enhancement is indeed a result of resonant photoionization, the wavelength of the excitation laser was varied between 493.00 nm and 500.00 nm. If there is a successful RELIBS measurement, the enhancement should be dependent on the wavelength and show a peak around 496.73 nm. Figure 4.5 shows the SNR of the Ti II peak as a function of the excitation wavelength.

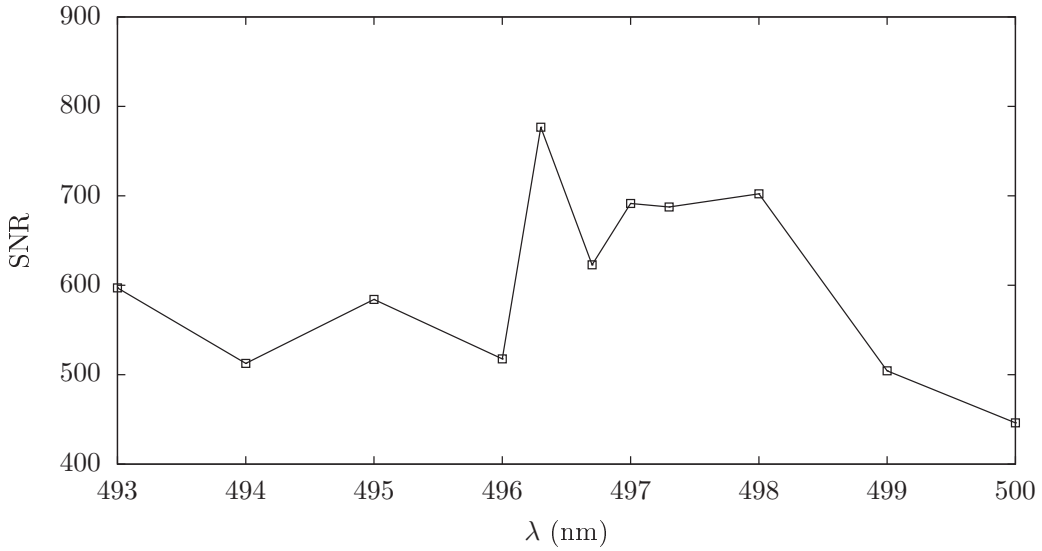

Figure 4.5: SNR of Ti II 453.40 nm peak as a function of excitation wavelength.

The wavelength of the excitation laser was checked by looking at a diffuse reflection of the laser. From the spectrum it appeared that the beam has two maximums, with an energy dip between them. The FWHM of the laser line was found to be 0.5 nm and the specified wavelength was roughly in the center.

From figure 4.5 it is apparent that there is clear dependence on the wavelength. The highest SNR is reached for an excitation wavelength of 496.3 nm. Taking the bandwidth and the two maxima of the excitation laser into account, this is within the line of expectation. Next to the peak at 496.3 nm a second peak is apparent with lower intensity. The reason for the extra peak between 497 nm and 498 nm in figure 4.5 is an extra photoionization wavelength in this region at 499.71 nm [17].

Figure 4.6 shows the intensity of the Al I peak as a function of the excitation wavelength, in the same fashion as for the Ti II peak. The Al I peak follows roughly the same path. It thus seems like the energy is indeed transferred to other elements in the sample, or at least to aluminum.

Judging from the strong wavelength dependence, the enhancement is indeed a result of resonant photoionization of the titanium species in the sample. Probably not all of the enhancement is a result of resonant photoionization, since also the off-resonant excitation wavelengths give an enhancement due to the double-pulse effect. Although this enhancement is less than with on-resonance excitation. Excitation with an off-resonance wavelength of 494.0 nm for example, gives the Al I peak at 396.15 nm a SNR of 92, compared to a SNR of 22 without excitation, a 4-fold enhancement.

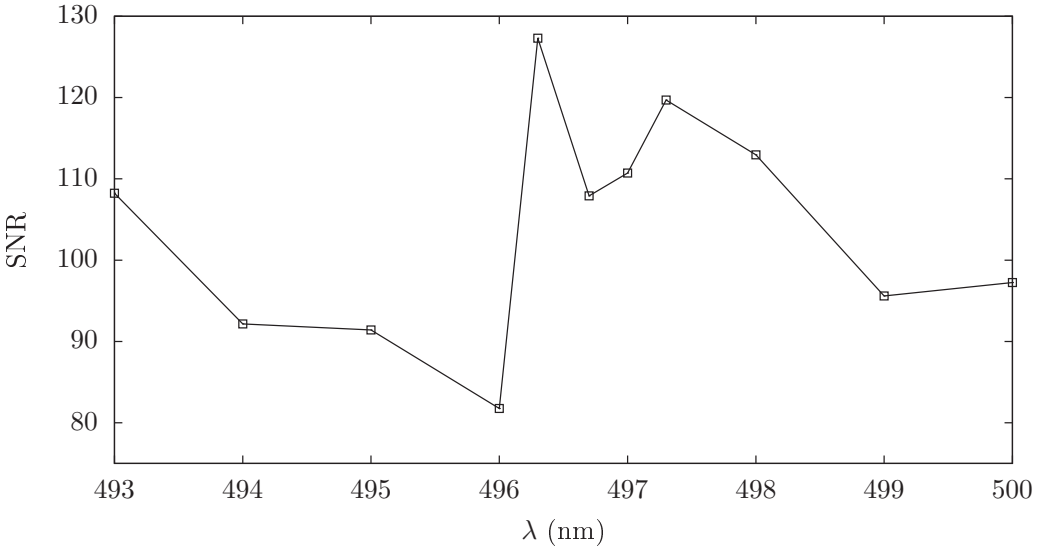

Figure 4.6: SNR of Al I 396.15 nm peak as a function of excitation wavelength.

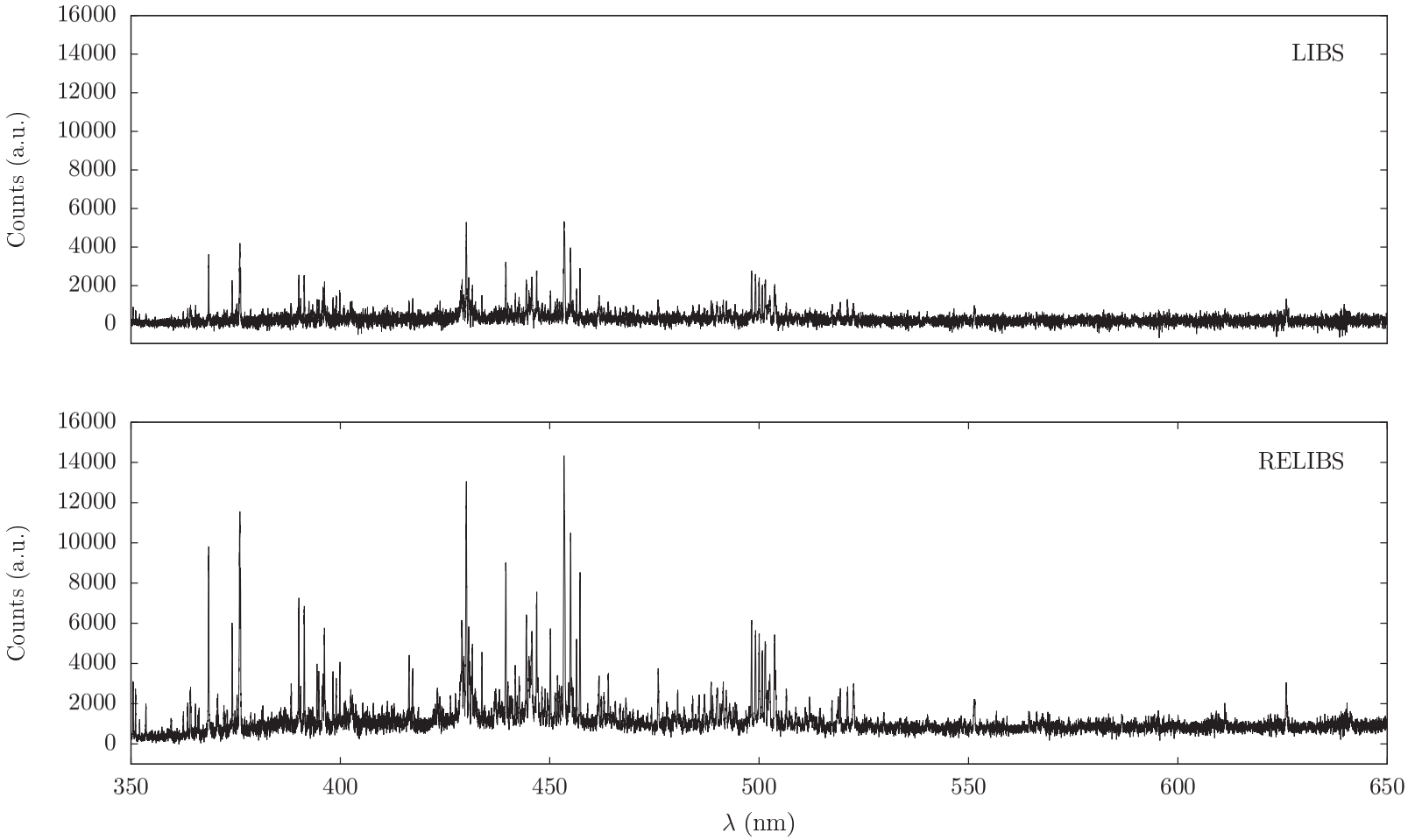

Figure 4.7: Comparison of RELIBS and LIBS spectra of titanium alloy. Note the overall increase in SNR and the appearance of new peaks around 560 nm.

Figure 4.8: The clipped beam profile (left) and unclipped beam profile (right).

Influences on the analytical performance of resonance-enhanced LIBS

In this subsection the influence of the beam profile, and the energy of the excitation and ablation laser on the analytical performance will be discussed. During the course of the research, the beam from the ablation laser appeared to be clipped. Although this was unintentional, it shows the consequences of a bad beam profile from the ablation laser on the performance of RELIBS very clearly. The results shown in this subsection are from the clipped ablation laser beam. RELIBS measurements were also carried out with the sample surface in the focus of excitation beam, causing the excitation beam to be ablation as well. Because some papers suggested that the RELIBS enhancement would be most prominent when energy of the ablation laser was just above the ablation threshold [13,14], the following measurements were performed with an attenuated ablation laser. The attenuation was done with the use of an ND-filter, as shown in figure 3.3.

Measurements were done on the same titanium alloy as in the previous section. The setting for the synchronization were the same. The differences in setup were: the attenuation of the ablation laser, the ablative power of the excitation laser and the clipped beam from the ablation laser. Figure 4.8 shows clipped laser beam profile compared to the unclipped laser beam on a piece of ablation paper. The paper was held just after the focusing lens. It is clear from figure 4.8 that the left beam profile is clipped.

Figure 4.9 shows both the RELIBS and the LIBS measurements. The spectra are averages of 50 measurements. Table 4.5 shows an overview of SNR's of the same peaks as in the previous subsection. The SNR of the Al I peak shows a 3-fold enhancement, while

Table 4.5: SNR ratio's for LIBS ions from titanium alloy spectrum.

Ion	Observed wavelength [nm]	LIBS SNR	RELIBS SNR
Al I	396.15	9	29
Ti II	453.50	37	150

the Ti II shows a 4-fold enhancement.

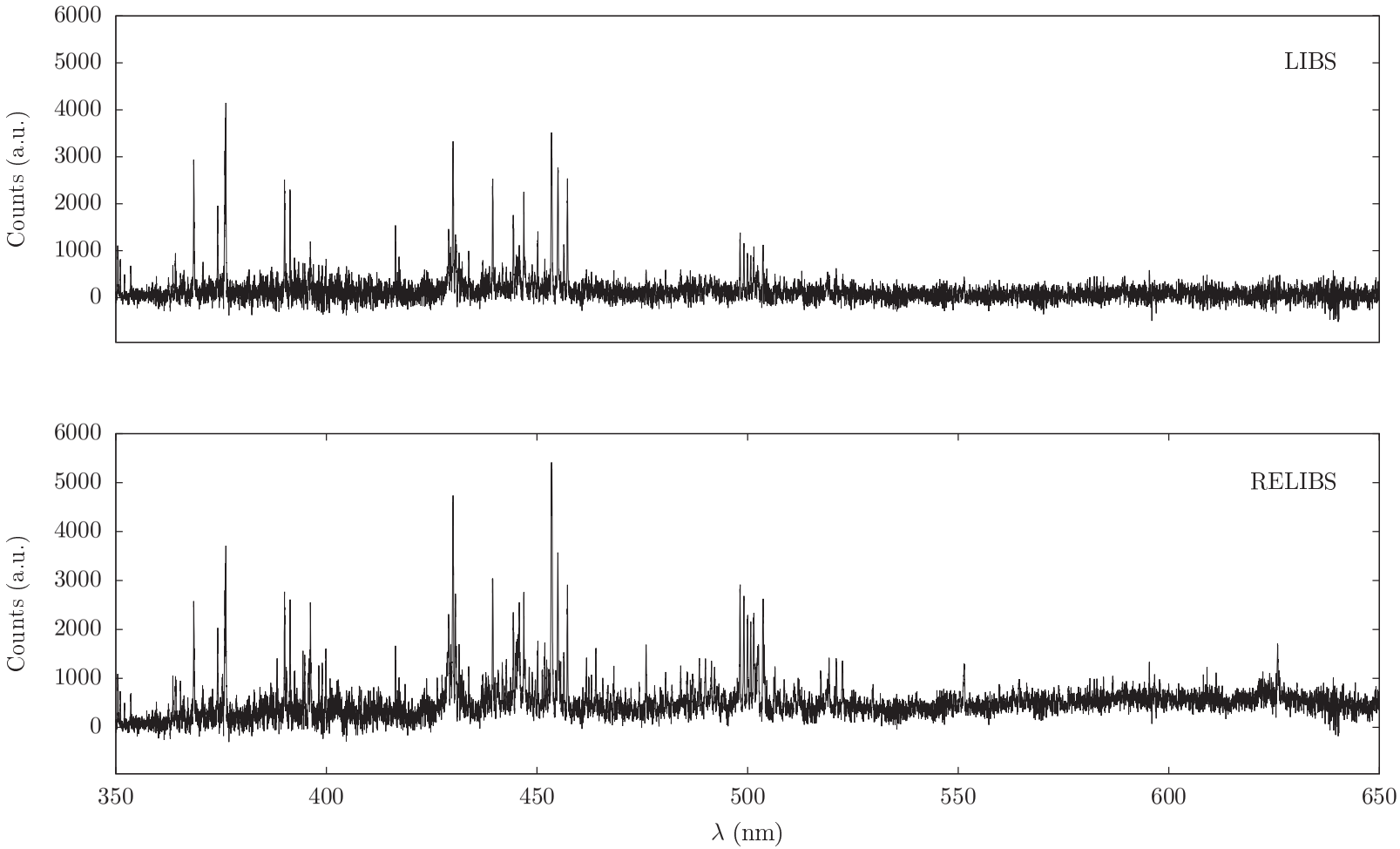

Figure 4.9: Comparison of RELIBS and LIBS spectra of titanium alloy. Note the increase in SNR and the appearance of new peaks around 560 nm.

However, in the enhanced signal, the continuum has also risen significantly. In figure 4.10 a zoomed in part of the two spectra are depicted together to make the increase of the continuum clearer. The black trace is the spectrum without excitation and the red trace is with excitation. This is a result of excitation laser causing a second ablation.

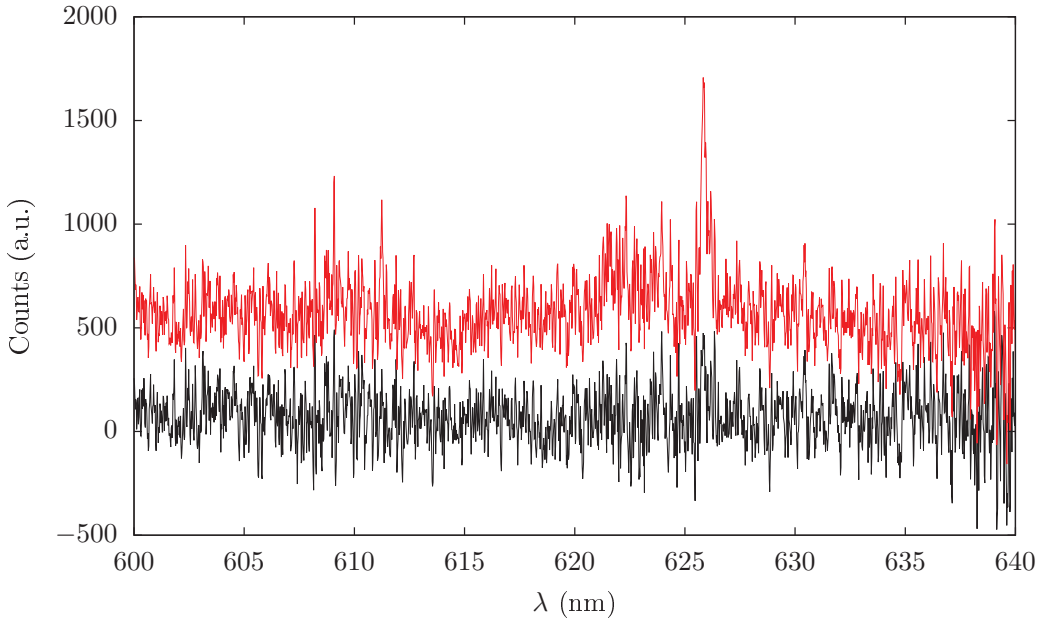

Figure 4.10: Part of titanium alloy spectrum. Black line: ablation without excitation laser, red line: ablation with excitation laser at 496.73 nm.

Figure 4.11 shows a picture of the two craters. This picture is taken by a camera with a microscope objective. The increase of the continuum is unwanted because this can diminish the resonant photoionization. Also apparent in this figure is that the crater from the ablation laser is not fully round, this is a direct result of the beam clipping.

To investigate if the enhancement is a result of resonant photoionization, the wavelength of the excitation laser was again varied. This time between 492.70 nm and 496.73 nm. Figure 4.12 shows the SNR of several peaks as a function of excitation wavelength. It is apparent from the figure that there is little dependence on the wavelength. All three peaks have roughly the same SNR for off-resonance wavelengths as for the on-resonance wavelength. This indicates that the enhancement in this case, is not a result of resonant photoionization.

The reason for the absence of resonance ionization is the combination of the clipped beam and the second ablation caused by the excitation laser. It is likely that most of the energy from the excitation laser was used to initiate a second plasma, which reheats the already 50 ns old plasma. Resonance enhancement from an ablating laser pulse tuned to a resonance wavelength is, with a few exceptions, unlikely. The tunable laser used in this research was too weak to investigate this properly. However, this case is investigated in literature [9]. Chang and Cheung used a tunable laser for a single-pulse LIBS measurement and reported no significant enhancement with on-resonance ablation compared to off-resonance ablation. Measurements with several different energies were done and

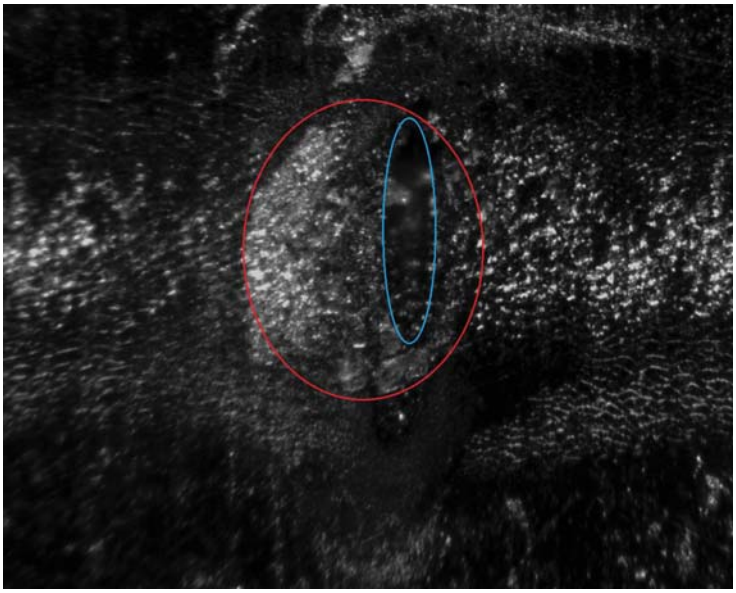

Figure 4.11: Image of overlapping carters (25x magnification). Red outline: crater from ablation laser, blue outline: crater from exciation laser. Also note that the crater from the ablation laser is not fully round because of the clipping.

the spectra remained independent of the wavelength of the laser. Their hypothesis is that in creating a plasma, thermal ionization dominates over other ionization channels, including photoionization. Any resonant photoionization that might be present, would make little difference.

To prevent a second ablation, the focal point of the laser beam from the excitation laser was moved into the sample, thus lowering the irradiance. This was done by simply moving the focusing lens (12 in figure 3.3). This also enlarges the diameter of the excitation beam and should make aligning easier. The RELIBS measurements were performed in the same fashion as with the previous setup, however, no enhancement was detectable. The reason for the lack of enhancement was most likely the clipped ablation beam profile. From research, also done by Cheung, it is apparent that RELIBS is very sensitive to the beam profile of the ablation laser [11]. According to the paper, a bad beam profile can make the resonant enhancement disappear completely. This is in agreement with the measurements performed during this research.

Steel alloy

Measurements with a low ablation threshold were also performed on a steel alloy (the full spectra of these measurement are not shown). The alloy was known to be either 304 or 316. The compositions of the two alloys is shown in table 4.6. After analyzing the spectrum of the steel alloy, two Molybdenum peaks were found: Mo I at 379.83 nm and Mo I at 390.30 nm. This indicates that the steel sample is made of alloy 316. This shows that LIBS can be used to identify the different types of alloys.

For the RELIBS measurement, the excitation wavelength was tuned to resonantly photoionize chromium at 428.97 nm [19]. Iron would be a better choice but the photoion-

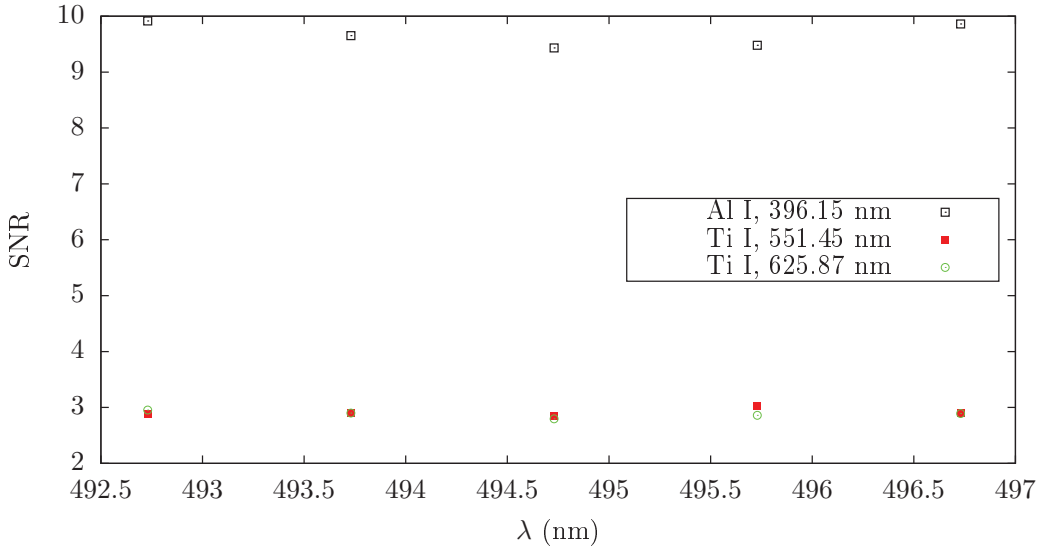

Figure 4.12: SNR of different titanium alloy peaks as a function of wavelength.

Table 4.6: Compositions of possible steel alloys [18].

Element	Alloy 304 [%]	Alloy 316 [%]
Carbon	≤ 0.08	≤ 0.08
Manganese	≤ 2.00	≤ 2.00
Phosporus	≤ 0.045	≤ 0.045
Sulfur	≤ 0.03	≤ 0.03
Silicon	≤ 1.00	≤ 1.00
Chromium	$\geq 18.00 \leq 20.00$	$\geq 16.00 \leq 18.00$
Nickel	$\geq 8.00 \leq 10.50$	$\geq 10.00 \leq 14.00$
Molybdenum	0	$\geq 2.00 \leq 3.00$
Iron	Remainder	Remainder

ization wavelengths for iron are between 270 nm and 306 nm [20], a region where the energy output of the excitation laser is too low (see figure 3.5).

Although an enhancement compared to the LIBS measurement was found, this was also no resonant enhancement because there was no wavelength dependency. The lack of resonant enhancement is not surprising because of relatively low concentration of chromium. However, something unexpected was found. Two LIBS peaks which were clearly present in the LIBS spectrum, disappeared almost completely in the RELIBS spectrum (see figure 4.13). Both peaks are from Fe I ions and appear at 393.36 nm and 396.92 nm. The reason for this fenomenon is unknown. A possible cause can be that the increased temperature increased the ionization in the plasma. A higher degree of ionization can mean that other transitions are more likely than the transitions that cause a 393.36 nm or 396.92 nm photon to be emitted. This effect is wavelength independent.

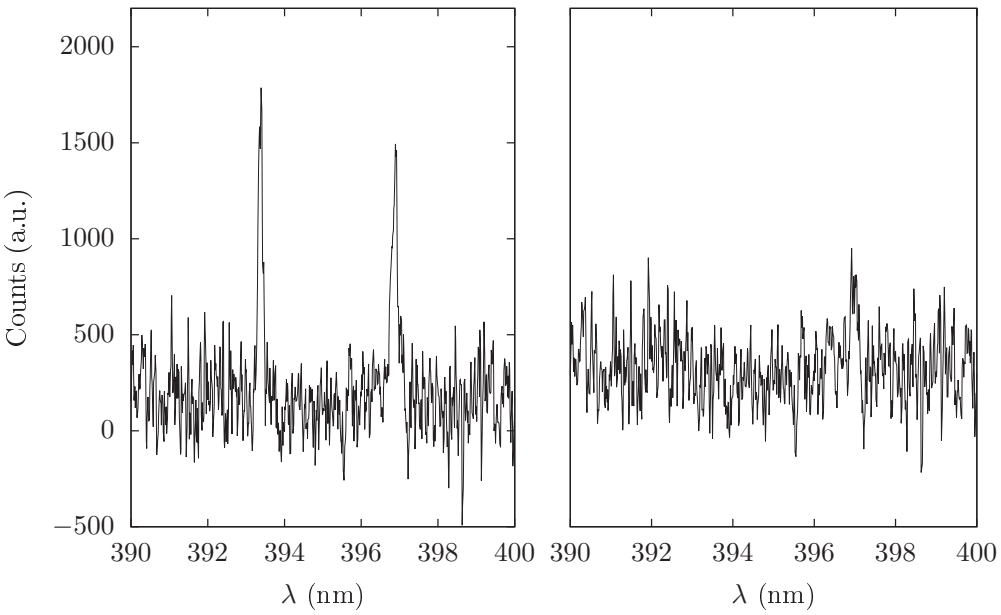

(a) Without excitation.

(b) With excitation at 428.97 nm.

Figure 4.13: Comparison of spectra from steel alloy.

5 Conclusion

The goal of this research was to determine if RELIBS is a practical way to improve the lower limit of detection of regular LIBS. A working RELIBS setup was realized. The titanium alloy showed a 7-fold enhancement for a Ti II peak at 453.40 nm and a 6-fold enhancement for a Al I peak at 396.15 nm. The enhancements that were visible were wavelength dependent, showing that the enhancement was indeed a result of resonance photoionization.

The RELIBS setup was found to be very sensitive. A second ablation caused by the excitation laser, diminished the resonant enhancement. As was clear by the increase of continuum and the lack of a dependence on the excitation wavelength. A bad beam profile will also prevent a RELIBS measurement from taking place. According to literature, good overlapping of the ablation and excitation laser is critical, a misalignment of a few hundred μm can prevent resonance photoionization.

A limiting factor during this research was the wavelength range in which the excitation laser has sufficient energy. This makes the number of RELIBS suitable materials limited. The excitation wavelengths studied in literature, are out of this range making direct comparison not possible. Because of invisible light from the excitation laser and the high energy, the alignment is also challenging.

In conclusion, RELIBS is a good method of enhancing LIBS measurements. This thesis showed great improvements, although even more improvement may be possible with an orthogonal setup (see recommendations). A drawback is the difficulty of building a proper setup and the high requirements for the excitation laser. With an off-resonance excitation wavelength a 4-fold enhancement was realized for the Al I peak. This indicates that a regular DB-LIBS setup is a good method of increasing LIBS performance if only a modest improvement is required.

6 Recommendations

If further research of RELIBS is desired, a few recommendations are suggested here.

Use a different excitation laser
A laser with more pulse energy at wavelengths between 200 nm and 400 nm is more suitable for RELIBS, since most the wavelength for photoionization of most common elements is in this range. Also, a laser with the same repetition rate as the ablation laser and a working external trigger can simplify the setup. A dye-laser is often used in literature and it's wide bandwidth makes this type of laser suitable for RELIBS.

Investigate materials from literature
When the excitation laser has higher pulse energies in the range of 200 nm and 400 nm, materials already investigated in literature come within reach. This makes direct comparison with literature possible and can aid in building a working setup.

Build an orthogonal setup
In an orthogonal setup the excitation laser overlaps with the plasma under a 90° angle. This can prevent ablation from the excitation laser and thus allows for higher pulse energies to be used, significantly increasing the enhancement. One paper found a 6 to 12 times higher SNR for an orthogonal setup [11].

Build an collinear setup
In a collinear setup, both laser pulses come onto the sample under the same angle. This makes alignment less difficult. With the current setup this was not practical, because the final mirror is a dichroic mirror optimized for the wavelength of the ablation laser. Also, the difference in wavelengths can cause the focal points of the two lasers to be at a slightly different position after the focusing lens. This misalignment might be too small to be a concern, but can be prevented by using a achromatic doublet to focus the beams instead of regular lens.

Even though RELIBS is more versatile than LIBS-LIF, it is still restricted by the excitation wavelength the abundant element in the sample. If, for example, an alloy of a different metal needs investigation, a different excitation wavelength is needed for the resonant photoionization. This problem can be solves by using a tunable laser, but these lasers are not common and often do not have the same energy output at every wavelength. Thus for RELIBS to be a good enhancement on LIBS, high requirements for the excitation laser are needed, or a limited range of materials must be acceptable.

If a more modest improvement in the LOD of LIBS is sufficient, a double-pulse LIBS setup might be a better choice. DP-LIBS requires a delay between the two lasers in the

range of microseconds instead of nanoseconds for RELIBS, which makes synchronization easier. DP-LIBS is also less sensitive for spacial misalignment of the two lasers. And an arbitrary wavelength can be used for the second laser pulse, making it as versatile as regular LIBS without the high requirements for the excitation laser.

Bibliography

[1] S. Maurice and R.C. Wiens. The chemcam instrument suite on the mars science laboratory (msl) rover: Science objectives and mast unit description. *Space Science Reviews*, 170(1-4):95–166, 2012.

[2] D.A. Cremers and L.J. Radziemski. *Handbook of Laser-Induced Breakdown Spectroscopy*. Wiley, 2006.

[3] J.P. Singh and S.N. Thakur. *Laser-Induced Breakdown Spectroscopy*. Elsevier Science, 2007.

[4] S. Laville, F. Vidal, M. Chaker, and M. Sabsabi. Laser-induced breakdown spectroscopy: investigation of pb resonant excitation and decay paths. *Industrial Applications of Optics: Materials Processing and Characterization*, 6343:634321–634321–8, 2006.

[5] V.I. Babushok, F.C. DeLucia Jr., J.L. Gottfried, C.A. Munson, and A.W. Miziolek. Double pulse laser ablation and plasma: Laser induced breakdown spectroscopy signal enhancement. *Spectrochimica Acta Part B: Atomic Spectroscopy*, 61(9):999 – 1014, 2006.

[6] F. Colao, V. Lazic, R. Fantoni, and S. Pershin. A comparison of single and double pulse laser-induced breakdown spectroscopy of aluminum samples. *Spectrochimica Acta Part B: Atomic Spectroscopy*, 57(7):1167 – 1179, 2002.

[7] S. Laville, C. Goueguel, H. Loudyi, F. Vidal, M. Chaker, and M. Sabsabi. Laser-induced fluorescence detection of lead atoms in a laser-induced plasma: An experimental analytical optimization study. *Spectrochimica Acta Part B: Atomic Spectroscopy*, 64(4):347 – 353, 2009.

[8] H. Loudyi, K. Rifai, S. Lavilleand F. Vidal, M. Chaker, and M. Sabsabi. Improving laser-induced breakdown spectroscopy (libs) performance for iron and lead determination in aqueous solutions with laser-induced fluorescence (lif). *J. Anal. At. Spectrom.*, 24:1421–1428, 2009.

[9] S. Y. Chan and N. H. Cheung. Analysis of solids by laser ablation and resonance-enhanced laser-induced plasma spectroscopy. *Analytical Chemistry*, 72(9):2087–2092, 2000.

[10] S.L. Lui and N.H. Cheung. Resonance-enhanced laser-induced plasma spectroscopy: ambient gas effects. *Spectrochimica Acta Part B: Atomic Spectroscopy*, 58(9):1613 – 1623, 2003.

[11] W.L. Yip and N.H. Cheung. Analysis of aluminum alloys by resonance-enhanced laser-induced breakdown spectroscopy: How the beam profile of the ablation laser and the energy of the dye laser affect analytical performance. *Spectrochimica Acta Part B: Atomic Spectroscopy*, 64(4):315 – 322, 2009.

[12] J. Scaffidi, S. M. Angel, and D. A. Cremers. Emission enhancement mechanisms in dual-pulse libs. *Analytical Chemistry*, 78(1):24–32, 2006.

[13] C. Goueguel, S. Laville, F. Vidal, M. Sabsabi, and M. Chaker. Investigation of resonance-enhanced laser-induced breakdown spectroscopy for analysis of aluminium alloys. *J. Anal. At. Spectrom.*, 25:635–644, 2010.

[14] S. L. Lui and N. H. Cheung. Minimally destructive analysis of aluminum alloys by resonance-enhanced laser-induced plasma spectroscopy. *Analytical Chemistry*, 77(8):2617–2623, 2005.

[15] A. Kramida, Yu. Ralchenko, J. Reader, and NIST ASD Team. Nist atomic spectra database. Online, 2012. Accessed: 2013-05-16.

[16] Ivea solution. IVEA LIBS: Limit of Detection in PPM. `http://www.ivea-solution.com/uploaded/images/ivea-wallpaper-1980-1024-Noir.jpg`. Accessed 2013-05-23.

[17] E.B. Saloman. A resonance ionization spectroscopy/resonance ionization mass spectrometry data service: Iv-data sheets for be, in, li, k, rb, ag, ti and v and an update of the data sheet for ni. *Spectrochimica Acta Part B: Atomic Spectroscopy*, 48(9):1139 – 1203, 1993.

[18] Bosun Supplies. Stainless steel info. `http://www.bosunsupplies.com/StainlessInfo2/`. Accessed 2013-05-28.

[19] E.B. Saloman. A resonance ionization spectroscopy/resonance ionization mass spectrometry data service. ii-data sheets for al, ca, cs, cr, co, cu, kr, mg, hg and ni. *Spectrochimica Acta Part B: Atomic Spectroscopy*, 46(3):319 – 378, 1991.

[20] E.B. Saloman. A resonance ionization spectroscopy/resonance ionization mass spectrometry data service. i-data sheets for as, b, cd, c, ge, au, fe, pb, si and zn. *Spectrochimica Acta Part B: Atomic Spectroscopy*, 45(1Ű2):37 – 83, 1990.

A Quantel Brilliant specifications and quality control.

QUANTEL

Brilliant

QUALITY CONTROL
Final Test Data Sheet

Model : Brilliant **Serial number :** W44

Repetition rate : 20 **Hz** **Cooling group :** Air/Water ⊘ Chiller ○

Energies :

Wavelength	Energy	Specs 10 Hz	Specs 20 Hz
1064 nm	360 mJ.	360 mJ	350 mJ
532 nm		180 mJ	160 mJ
355 nm		65 mJ	60 mJ
266 nm		40 mJ	30 mJ

Flashlamp discharge voltage : 1320 **V**

Pulse duration (FWHM) @ 1064nm : 4,00 **ns**

Far field pattern @ 1064nm shown on attached page

Burn pattern (30 cm)

λ = 1064nm

GENERAL OPERATION CONTROL

RS232 : ⊘
External flashlamp trigger : ⊘
External Q-Switch : ⊘
Security interlocks : ⊘
(FHG option) T° parameter : /

Date : 21/12/98 **Tested by :** M. Narbonnaud.

Brilliant

Compact Q-Switched Nd : YAG oscillator with super gaussian resonator

Beam diameter : 6mm - 1 flashlamp - air/water heat exchanger - interchangeable harmonic generators

Beam profile in near field @ 1064 nm, 10 Hz

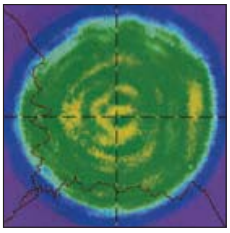

Beam profile in far field @ 1064 nm, 10 Hz

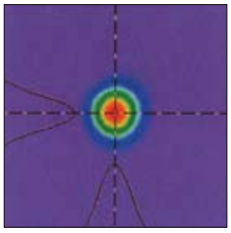

Beam profile in far field @ 532 nm, 10 Hz

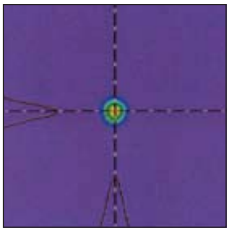

Temporal profile @ 1064 nm, 10 Hz

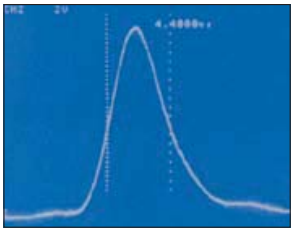

Horizontal Cursor Profile

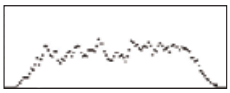

Horizontal Cursor Profile

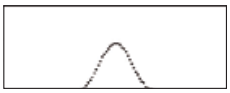

Horizontal Cursor Profile

Vertical Cursor Profile

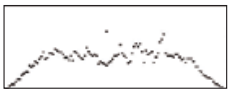

Vertical Cursor Profile

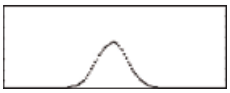

Vertical Cursor Profile

Optical laser head :	5 kg	(11.02 lb)
(H x L x W)	136 x 469 x 80	(5.35 x 18.46 x 3.15)
Power supply and cooling group cabinet :	55 kg	(121 lb)
(H x L x W)	585 x 592 x 286	(23.03 x 23.3 x 11.26)
Harmonic generation module including separation package (each) :	2,1 kg	(4.63 lb)
(H x L x W)	118 x 158 x 78	(4.65 x 6.2 x 3.07)
Remote control (foot print)	195 x 100	(7.68 x 3.94)

All dimensions are in mm (inch).

External synchronization flexibility : flashlamp external control through TTL signal or RS232 interface ; Q-Switch external control through TTL signals, RS232 interface or remote box. **Reduced warm up-time :** heating element in coolant reservoir.

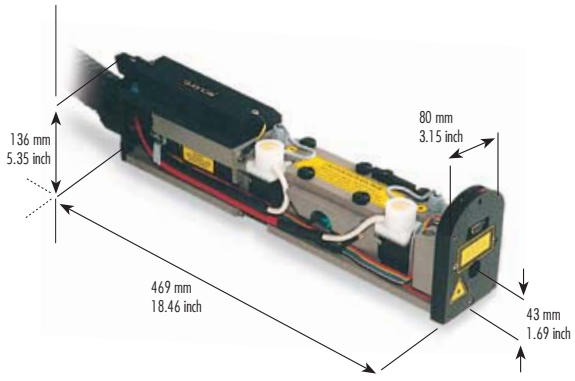

Brilliant Specifications

Repetition rate (Hz)		10	20	50	
Energy per pulse (mJ)	1064 nm	360	350	150	Measured with a calibrated wattmeter
	532 nm	180	160	65	
	355 nm	65/100*	60/70*	20	*High energy UV option
	266 nm	40	30	12	
	213 nm	8	6	2	
Energy stability - shot to shot (%)	1064 nm	±2 (0.6)	±2 (0.6)	±3 (1)	Peak to peak, 100% of the shots (RMS)
	532 nm	±4 (1.3)	±4 (1.3)	±7 (2.3)	
	355 nm	±6 (2)	±6 (2)	±9 (3)	
	266 nm	±8 (2.6)	±8 (2.6)	±12 (4)	
	213 nm	±12 (4)	±12 (4)	±16 (5.3)	
Power drift (%)	1064 nm	±3	±3	±3	Over 8 hours, without readjustment of
	532 nm	±3	±3	±3	phase-matching, 18°C<T°<28°C (10Hz/20Hz)
	355 nm	±3	±3	±3	18°C<T°<25°C (50Hz)
	266 nm	±6	±6	±6	W/W exchanger or chiller options available
	213 nm	±10	±10	±10	
Pulse duration (ns)	1064 nm	≈5	≈5	≈6	FWHM, fast photodiode and 1GHz scope
	532 nm	≈4	≈4	≈5	
	355 nm	≈4	≈4	≈5	
	266 nm	≈4	≈4	≈5	
	213 nm	≈4	≈4	≈5	
Linewidth (cm-1)	1064 nm	0.7	0.7	0.7	FWHM, measured by a grating
	532 nm	1.4	1.4	1.4	spectrometer with a 0,045 cm^{-1} resolution
Jitter (ns)	1064 nm	±0.5	±0.5	±0.5	With respect to Q-switch trigger, measured at half-width of 500 accumulated shots
Pointing stability (µrad)	1064 nm	<50	<75	<75	Measured by SPIRICON LBA-100,
	532 nm	<50	<75	<75	RMS, on 200 pulses at the focal plane
	355 nm	<50	<75	<75	of a 2m focus lens
	266 nm	<50	<75	<75	
Divergence (mrad)	1064 nm	0.5	0.5	0.7	Full angle, at $1/e^2$ of the peak, 85 % of total energy
Polarization ratio (%)	1064 nm	>90	>90	>80	Horizontal polarization
Beam diameter (mm)	1064 nm	6	6	6	At the output of the laser
Focusability (times Diffraction Limit)	1064 nm	<2	<2	<3	At $1/e^2$ of the peak, by SPIRICON LBA-100
Spatial profile (fit to gaussian)					
Near field	1064 nm	0.70	0.70	0.70	At 1m from the laser output
Far field	1064 nm	0.95	0.95	0.90	At focal plane of a 2m focus lens
					Least square fit to gaussian (perfect fit=1)

Double pulse option is available. Contact us for more information.

Service requirement Power : 100-240V, 10A, 50/60Hz
Cable length : 3 m (10 feet)

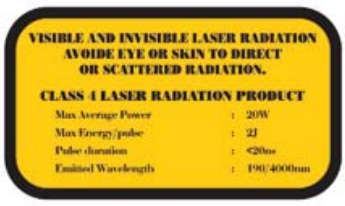

2 bis, Avenue du Pacifique - ZA de courtaboeuf - BP 23 - 91941 Les Ulis Cedex - France
Tel : + 33 (0)1 69 29 17 00 - Fax : + 33 (0)1 69 29 17 29 - email : quantel@quantel.fr - www.quantel-laser.com
Quantel - USA : 601 Haggerty Lane - Bozeman, MT 59715 - 2001 - USA - Tel : + 1 406 586 0131 - fax : + 1 406 586 2924

B Specifications Ekspla NT242-SH Tunable Diode Pumped Laser System

STANDARD SPECIFICATIONS

Pump laser requirements

Wavelength	**355 nm**
Pulse width	~ 7 ns
Pulse energy	< 3 mJ
Pulse energy stability	2.5%
Pulse repetition rate	1000 Hz
Beam diameter (full width at 0.1 level)	~ 0.8 mm
Beam divergence	< 3 mrad (full angle @1/e^2)
Beam profile	TEM_{00}
Polarization	vertical
Jitter (with respect to internal SYNC pulse)	± 1 ns
Beam profile	Close to Gaussian

OPG output specification

Tuning range:	355 nm, 210 – 399.9 nm 400 – 709.9 nm, 710 – 2500 nm
Pulse energy	Max 1 mJ
Pulse duration	~ 7 ns
Max. conversion efficiency	~ 15%
Polarizations:	
355 nm	Vertical
210 – 399.9 nm	Vertical
400 – 709.9 nm	Horizontal
710 – 2500 nm	Vertical
Output beam mode	Elliptical

OPG general specification

Power	90-240 VAC, 50/60 Hz
Required power	< 1000 W
Dimensions:	
NT242	445×800×230 mm
PS611800 power supply	392×365×288 mm
Weight	
NT242	~50 kg
PS611800 power supply	~20 kg

C | Specifications Highland T564 digital delay and pulse train generator

Specifications : T564 advanced digital delay and pulse train generator

FUNCTION	4-channel digital delay and pulse generator
GATE FUNCTION	Programmable as level sensitive enable input, edge triggered burst enable input, or divisor enabled output
GATE INPUT	Programmable termination, 50Ω or 500Ω to +2.5 V Logic low -0.3 V min, +0.7 V max Logic high +2 V min, +5 V max
GATE OUTPUT	Logic low +0.1 V typical, +0.4 V max @ 50 mA Logic high +5 V typical, +4 V min @ 50 mA
TRIGGER SOURCES	Internal DDS: 0 to 16 MHz, 0.02 Hz resolution Internal clock: 80 MHz Remote command or External signal
TRIGGER DIVISOR	1 to 2^{32}-1, 125 MHz max input
EXTERNAL TRIGGER INPUT	Programmable termination, 50Ω or 10 kΩ to ground Programmable trigger level (+0.25 to +3.3 volts) and slope
CHANNEL OUTPUTS A, B, C, D	Four pulse outputs, 5 V, 50Ω source impedance, each programmable for delay, width, polarity
DELAY RANGE	0 to 10 seconds, 10 ps resolution
WIDTH RANGE	2 ns to 10 seconds, 10 ps resolution
INSERTION DELAY	20 ns ±400 ps, external trigger to any output
DIFFERENTIAL NONLINEARITY	< 200 ps
JITTER	< 35 ps typical (50 ps max) RMS, external trigger to any output or between any outputs Add clock jitter for delays > 500 µs
TRIGGER RATE	0 to 16 MHz, limited to 1/(delay+width+60 ns) max
RISETIME	750 ps max
CLOCK	Internal 10 MHz VCXO, 1 ppm initial accuracy, < 2 ppm/year drift Added jitter below 10 ns per second of delay TC below 0.2 PPM/°C Connector provides clock in/out Locks to external source Clock jitter and delay errors are zero relative to external source Optional higher-performance TCXO or OCXO
TIMING ACCURACY	±400 ps ±7.5 ps/°C ±clock accuracy
BURST	Programmable to fire N times out of each M triggers where N and M are 1 to 2^{32}-1
OPERATING TEMPERATURE	0 to 50°C, non-condensing
STORAGE TEMPERATURE	-20 to 80°C
POWER	+12 ±0.25 volts, 0.3 amps max; 0.4 amps max with Ethernet Universal AC adapter supplied with evaluation package
COMMUNICATIONS	RS-232 standard, 38.4 kbaud Optional 10/100 Ethernet
CONNECTORS	7 SMB for trigger, gate, clock, outputs 2.5 mm stereo jack for RS-232 0.25" power connector Optional RJ45 for Ethernet
PACKAGING	4.75" (L) x 4.0" (W) x 1.25" (H) extruded aluminum enclosure
CONFORMANCE	OEM product has no UL/FCC/CE compliance requirements Designed to meet UL/FCC/CE requirements

18 Otis Street San Francisco, CA www.HighlandTechnology.com tel: 415 551-1700 fax: 415 551-5129

D Adapted Matlab function for Highland settings

```
function [ReturnString, BytesRead] = ...
    HIGHLANDT564_SelectTrigger(DeviceNumber, TriggerMode, RepRate, ...
    PulseNumber, MaximumLength, TriggerRepRate)
% This function uses library OMILAB.DLL for communication. This DLL ...
    with h-file are loaded with matlab m-file OMILOAD.m. This function ...
    can be inserted at the top of each file that uses OMILAB functions.

    % Load OMILAB
    OMILAB_Load;

    % Some variables
    BytesRead = -1;
    DefaultMaximumLength = 80;
    trigger_type_cw = 1;
    trigger_type_train = 2;
    trigger_type_external = 3;

    % Check for valid number of parameters
    if (nargin < 3)
        disp('[ReturnString, BytesRead] ...
            =HIGHLANDT564_SelectTrigger(DeviceNumber, TriggerMode, ...
            RepRate, [PulseNumber], [MaximumLength])');
        return ;
    end

    % Communication with the Highland
    Parameters = HIGHLANDT564_Parameters();
    if ((DeviceNumber < 1) || (DeviceNumber > ...
        Parameters.MaximumDeviceNumber))
        disp(['DeviceNumber out of valid range [1 - ' ...
            num2str(Parameters.MaximumDeviceNumber, '%0d') ']']);
        return;
    end
    if (Parameters.Device(DeviceNumber).PortHandle < 0)
        disp(['Device not connected i.e. no valid porthandle: ' ...
            num2str(Parameters.Device(DeviceNumber).PortHandle, '%0d')]);
        return;
    end

    % Define trigger mode
    if strcmpi(TriggerMode,'cw')
```

```
33          TriggerMode=trigger_type_cw;
34      elseif strcmpi(TriggerMode,'train')
35          TriggerMode=trigger_type_train;
36      elseif strcmpi(TriggerMode,'external')
37          TriggerMode=trigger_type_external;
38      else
39          disp(['Only values ''cw'', ''train'' and ''external'' admitted ...
                for variable TriggerMode']);
40          return;
41      end
42      Port = Parameters.Device(DeviceNumber).PortAddress;
43      ConnectType = Parameters.Device(DeviceNumber).PortTypeNumber;
44
45      if (nargin ≥ 5)
46          if(length(MaximumLength) > 0)
47              if (MaximumLength > 0)
48                  DefaultMaximumLength = MaximumLength;
49              end
50          end
51      end
52
53      %Select trigger mode
54      switch(TriggerMode)
55          case trigger_type_train;
56              Divider=ceil((1/RepRate)/20e-9); Npulse=PulseNumber-1;
57              AsciiString=strvcat('TR of;', strcat('TS ...
                    ',num2str(Divider),';','TC ',num2str(Npulse),'; TR RE; ...
                    in; Fire;'));%String with commands that will be send ...
                    to configure the Highland
58              CommCont = length(AsciiString(:,1));
59              for i=1:CommCont
60              BytesSend = SERIAL_WriteAscii(Port, AsciiString(i,:));
61              pause(0.5);
62              end
63          case trigger_type_cw;
64              AsciiString=strcat('TC 0; SY ',num2str(RepRate), ';TR SY; ...
                    In;');%String with commands that will be send to ...
                    configure the Highland
65              %Sets pulse train to 0, enable trigger by SY with user set
66              %reprate.
67              BytesSend = SERIAL_WriteAscii(Port, AsciiString);
68          case trigger_type_external;
69              Divider = ceil((1/RepRate)/20e-9);
70              TriggerDivider = TriggerRepRate/RepRate;
71              Npulse=PulseNumber-1;
72              AsciiString=sprintf('TR of; TC off; TD %d;BU of;ga in;ga ...
                    re;tr po;ts %d;tc %d;ga fi', TriggerDivider, Divider, ...
                    Npulse) %String with commands that will be send to ...
                    configure the Highland
73              BytesSend = SERIAL_WriteAscii(Port, AsciiString);
74      end
75          if (BytesSend < length(AsciiString))
76          ReturnString = '';
77          error('Error: not able to send bytes');
78      end
79      ReturnString = char(32*(ones(1,DefaultMaximumLength+1)));
80      [ReturnString, BytesRead] = SERIAL_ReadAscii(Port, ...
            DefaultMaximumLength);
81  return
```

E | Matlab script for measurements

```
%%%%%%%%%%%%%%%%%%%%%%%%%%%%%%%%%%%%%%%%%%%%%%%%%%
% Software to perform a measurement.
% All times in seconds, all linear dimensions in mm!
% HIGHLAND is controlled using RS232 interfaces.
% %%%%%%%%%%%%%%%%%%%%%%%%%%%%%%%%%%%%%%%%%%%%%%%%%

%% Clean up
HIGHLANDT564_Close(1);
ESP300_Close(2);
clear all
close all
clc

%% User input for sample and scan parameters
chk_numspectra = 25; %Number of measurements to take
chk_pulsepermeasurement = 1; % Number of pulses to shoot per site
chk_reprate_high = 1002;
chk_reprate_low = 20; % Laser rep rate. Should be fixed to 20 Hz
chk_divider = chk_reprate_high./chk_reprate_low;

% Laser and ICCD
chk_gatedelay = -15e-9;% Gate delay in seconds.
chk_interdelay = 50e-9; % Delay between ablation laser and excitation ...
    laser
chk_openingMCP = 30e-6; % Opening interval for MicroChannelPlate. It ...
    will be identical to the one for the laser
chk_gatedelay = chk_gatedelay + 0.865e-6;% Correction for Brilliant ...
    delay. 0.805u for Qsdelay of 200u, 0.845u for Qsdelay of 128u

% Translation stage
chk_motorpositionsxstart = 3;    %Start X position (axis 1) [mm](≥3)
chk_motorxstepsize = 0.75; % Distance between 2 consecutive ...
    measurements in the x axis [mm]
chk_motorxlength = chk_numspectra; % Total scan distance in x axis [mm]
motorpositionsx = (chk_motorpositionsxstart:chk_motorxstepsize: ...
    (chk_motorpositionsxstart+(chk_motorxlength-1)* ...
    chk_motorxstepsize)); % Motor position x

%% Fixed parameters
ekspla_delay = 211.66e-6; %Time between rising edge of sync out and ...
    laser pulse (Ekspla triggers at falling edge), full power: ...
```

```
    211.66e-6, 113us: 208.75e-6
qsdelay= 200e-6; %Q-switch delay Brilliant laser
CCDintegration_delay= 0;
openinglaser= 10e-6; %Laser is programmed to shoot after 10 us after ...
    the opening of the CCD.

%% Check if timing is possible
if (ekspla_delay-chk_interdelay-qsdelay-openinglaser) < 0
    disp('Impossible timing')
    break
end

%% Connection and initialization of delay generator and stage controller

% Highland Digital Delay Generator
highlanderror=HIGHLANDT564_SerialConnect(1,8); %Assigned device #1 to ...
    DDG which should be in COM 4
if highlanderror~=0
    'Highland communication error'
    return
end

% ESP 300 stage controller
if check_results.nummeasurement ~= 1
    esperror=ESP300_Connect(2,'serial', 7); %Assigned device# 2 to ...
        motor which should be in COM 5
    if esperror<0
         'ESP communication error. Restart ESP300 and try again'
        return
    end
end
pause(1);

%% Initialization of DDG channels and translation stage

% Highland
HIGHLANDT564_InitializeChannel(1,'A', ...
    (ekspla_delay-chk_interdelay-qsdelay),50e-6); % Flashlamp ablation ...
    laser
HIGHLANDT564_InitializeChannel(1,'B', ...
    (ekspla_delay-chk_interdelay)+check_results.trigger.gatedelay ...
    ,check_results.trigger.openingMCP); % Gate camera
HIGHLANDT564_InitializeChannel(1,'C', ...
    (ekspla_delay-chk_interdelay-openinglaser)+CCDintegration_delay, ...
    check_results.trigger.openingMCP.*2); % Trigger camera
HIGHLANDT564_InitializeChannel(1,'D', ...
    (ekspla_delay-chk_interdelay),50e-6); % Q-switch ablation laser

% ESP300
if check_results.nummeasurement ~= 1
    ESP300_SetHome(2,1); %Set home position, corresponding to zero
    ESP300_SetPosition(2,1,chk_motorpositionsxstart);
        Motion = ESP300_Motion (2,1);
        while Motion==1
        Motion = ESP300_Motion (2,1);
        end
end

%% Measurement
```

```
loop=0;
for i=1:check_results.nummeasurement;
    loop=loop+1;
    disp(['Loop ' num2str(loop) ' out of ' ...
        num2str(check_results.nummeasurement) ]);

    % ESP300
    if check_results.nummeasurement ≠ 1
        ESP300_SetPosition(2,1,check_results.motorpos.x(i));
            Motion = ESP300_Motion (2,1);
            while Motion==1
            Motion = ESP300_Motion (2,1);
            end
    end
    pause(1)

    % Highland
    [read,bites]=HIGHLANDT564_SelectTrigger2(1,'external',chk_reprate_low,check_results.tri
        [],chk_reprate_high);
    pause(0.5 + chk_pulsepermeasurement/chk_reprate_low);
end

HIGHLANDT564_Close(1);
ESP300_Close(2);
disp('Measurement finished')
```

F | Specifications LTB Lasertechnik Berlin ARYELLE 200

Spectrometers

Specifications ARYELLE 200, typ.

Aperture	f/10
Focal length	200 mm
Slit width	40 µm
Wavelength range	220 - 800 nm / 200 - 750 nm
Spectral resolving power	9,000
Spectral resolution	24 - 90 pm / 22 - 83 pm
Crosstalk	5×10^{-3} (ICCD) / 2×10^{-3} (CCD) measured @ 253.652 nm and full slit height
Straylight	1×10^{-4}
Detector	CCD/ICCD 1,024 x 1,024 pixels, 13 x 13 mm^2 image area
Dynamic range	15 bit, AD conversion 16 bit
Light coupling	SMA-fibre coupling
Wavelength calibration	With Hg lamp
Absolute accuracy	Spectral resolution/4
Computer	PC or laptop with Windows
Software	Sophi
Dimensions without detector (L x W x H)	(260 x 160 x 185) mm, (10.24 x 6.3 x 7.28) in
Weight without detector	7.3 kg (16.0 lbs)

other spectral resolutions and wavelength ranges are possible

LTB Lasertechnik Berlin GmbH • Rudower Chaussee 29 • D-12489 Berlin • Germany
Telefon: +49.30.63 92-61 90 • Telefax: +49.30.63 92-61 99 • E-mail: info@ltb-berlin.de • www.ltb-berlin.de

State: 1.5.2011

G | Specifications Andor iStar ICCD

2.4 - CCD PLATFORM SPECIFICATIONS - SPECTROSCOPY SENSORS

MODEL	320T		340T	
Total CCD matrix size (pixels)	1024 x 255		2048 x 512	
Fibre optic taper magnification (std)	Ø 18 mm II 1:1	Ø 25 mm II 1:1	Ø 18 mm II 1:1	Ø 25 mm II 1:1
Effective CCD pixel size	26 x 26 µm 100% fill factor		13.5 x 13.5 µm 100% fill factor	
Effective active area	18 x 6.7 mm	25 x 6.7 mm	18 x 6.9 mm	25 x 6.9 mm
Image pixel well depth	500,000 e^-		100,000 e^-	
Register well depth	550,000 e^-		150,000 e^-	
Read noise (e^-) 50 kHz 1 MHz 3 MHz 5 MHz	 7 [9] 12 [13] 19 [20] 25 [32]		 6 [8] 9 [12] 12 [18] focussing mode only	
Maximum frame and spectral rates				
Frame [2 x 2 binning] Crop mode (frame, 10 rows)	15.9 fps [28.9 fps] 320 fps		2.5 fps [5.6 fps] 184 fps	
FVB Crop mode (spectrum, 10 rows)	322 sps 2,941 sps		135 sps 1,825 sps	
Fast Kinetics 4 rows 2 rows	 16,610 Hz 26,590 Hz		 16, 950 Hz -	
Sensitivity	2 to 10 e^-/count (software selectable)		1 to 5 e^-/count (software selectable)	
Linearity	Better than 99%			
Minimum temperature air cooled [dark current, e^-/pixel/sec]	Ø 18 mm II -30°C [0.4]		Ø 18 mm II -30°C [0.2]	Ø 25 mm II -25°C [0.4]
Coolant chiller, coolant @ 10°C, 0.75 l/min [dark current, e^-/pixel/sec]	-40°C [0.12]		-40°C [0.1]	-35°C [0.15]

Note: All specifications are typical unless otherwise stated

H | Original project description

Soil contamination determination using Raman-LIBS spectroscopy

Goal

The goal of the project is to investigate the possibilities of using Raman and LIBS (Laser Induced Breakdown Spectroscopy) techniques in determining the pollutant contamination of soils.

Motivation

Soil contamination around factories remains a large problem, especially for nano-particles fabrication environments. An example is the contamination with carbon nanotubes, where the pollution is considered substantial only when the short length carbon nanotubes are present. Using spectroscopy techniques, the presence and length of the carbon nanotubes can be investigated in embedded in soil with ppm (parts-per-milion) concentrations. Raman and LIBS spectroscopy are suitable to detect the molecular and elemental composition of a sample.

Activities:

This project will focus on implementing Raman and LIBS spectroscopy to detect the presence of carbon-nanotubes and other pollutants (as Pb, Cu) in soils. Project activities will focus on:

- Investigate the detection possibility of contaminant using Raman and LIBS by direct measurements
- Experimental determination of limit of detection of various molecules and atoms
- Improvement of detection limit using double-pulsed LIBS (two lasers instead of one as currently used)
- Data analysis and interpretation of spectra
- Writing a report presenting the problem, technique and results

Duration: 4 months
Student: Daniel Bouman
Supervisor: Maria Sovago